

Article

Development and In Vitro Characterization of [³H]GMC-058 as Radioligand for Imaging Parkinsonian-Related Proteinopathies

Andrea Varrone ^{1,*}, Vasco C. Sousa ², Manolo Mugnaini ³, Sandra Biesinger ⁴, Gunnar Nordvall ⁵, Lee Kingston ⁶, Ileana Guzzetti ⁷, Charles S. Elmore ⁶, Dan Sunnemark ^{8,9}, Dinahlee Saturnino Guarino ¹⁰, Sjoerd J. Finnema ¹¹ and Magnus Schou ¹²

- ¹ Department of Clinical Neuroscience, Centre for Psychiatry Research, Karolinska Institutet and Stockholm Health Services, BioClinicum, J4-14, Akademiska Stråket 1, 17176 Solna, Sweden
 - ² Department of Clinical Neuroscience, Division of Imaging Core Facilities, Karolinska Institutet, Stockholm, Sweden, BioClinicum, J5, Akademiska Stråket 1, 17176 Solna, Sweden; vasco.sousa@ki.se
 - ³ Translational Sciences, Neuroscience & Ophthalmology Discovery Research, AbbVie Deutschland GmbH & Co., KG, Knollstraße 50, 67061 Ludwigshafen, Germany; manolo.mugnaini@abbvie.com
 - ⁴ Advanced Cell Technologies & Screening, Neuroscience & Ophthalmology Discovery Research, AbbVie Deutschland GmbH & Co. KG, Knollstraße 50, 67061 Ludwigshafen, Germany; sandra.biesinger@abbvie.com
 - ⁵ AlzeCure Pharma AB, Hälsovägen 7, 14157 Huddinge, Sweden; gunnar.nordvall@alzecure.org
 - ⁶ Isotope Chemistry, Early Chemical Development, Pharmaceutical Sciences, R&D, AstraZeneca, Pepparedsleden 1, 43183 Mölndal, Sweden; lee.kingston@astrazeneca.com (L.K.); chad.elmore@astrazeneca.com (C.S.E.)
 - ⁷ Medicinal Chemistry, RIA, Biosciences R&D, AstraZeneca, Pepparedsleden 1, 43183 Mölndal, Sweden; ileana.guzzetti@astrazeneca.com
 - ⁸ Offspring Biosciences, Forskargatan 20 J, 15136 Södertälje, Sweden; dan.sunnemark@offspringbiosciences.se
 - ⁹ Department of Clinical Neuroscience, Karolinska Institutet, Center for Molecular Medicine, Karolinska University Hospital, 17176 Stockholm, Sweden
 - ¹⁰ Department of Radiology, Perelman School of Medicine, University of Pennsylvania, 1012, 231 S. 34th Street, Philadelphia, PA 19104, USA; dinahlee.saturninoguarino@pennmedicine.upenn.edu
 - ¹¹ Translational Sciences, Neuroscience & Ophthalmology Discovery Research, AbbVie, 1 North Waukegan Road, North Chicago, IL 60064, USA; sjoerd.finnema@abbvie.com
 - ¹² Precision Medicine Diagnostic Development and HBS Science, AstraZeneca R&D Oncology, AstraZeneca J4:14, BioClinicum, Akademiska Stråket 1, 17176 Solna, Sweden; magnus.schou@astrazeneca.com
- * Correspondence: andrea.varrone@ki.se



Academic Editor: Francesco Gubellini

Received: 4 April 2025
Revised: 18 May 2025
Accepted: 3 June 2025
Published: 9 June 2025

Citation: Varrone, A.; Sousa, V.C.; Mugnaini, M.; Biesinger, S.; Nordvall, G.; Kingston, L.; Guzzetti, I.; Elmore, C.S.; Sunnemark, D.; Saturnino Guarino, D.; et al. Development and In Vitro Characterization of [³H]GMC-058 as Radioligand for Imaging Parkinsonian-Related Proteinopathies. *Cells* **2025**, *14*, 869. <https://doi.org/10.3390/cells14120869>

Copyright: © 2025 by the authors. Licensee MDPI, Basel, Switzerland. This article is an open access article distributed under the terms and conditions of the Creative Commons Attribution (CC BY) license (<https://creativecommons.org/licenses/by/4.0/>).

Abstract: The molecular imaging of α -synuclein (α -syn) pathology in Parkinson's disease (PD) and related movement disorders is a clinically unmet need. The aim of this study was to discover and characterize in vitro a radioligand for imaging α -syn pathology. A library of 78 small molecules was developed and screened using recombinant α -syn fibrils and brain homogenates from Alzheimer's disease (AD) donors. The selection criteria were as follows: $K_{i\alpha\text{-syn}} < 30$ nM, $K_{i\text{tau}}$ and $K_{iA-\beta} > 200$ nM. Three compounds, GMC-073 ($K_{i\alpha\text{-syn}}$: 8 nM), GMC-098 ($K_{i\alpha\text{-syn}}$: 9.7 nM), and GMC-058 ($K_{i\alpha\text{-syn}}$: 22.5 nM), fulfilled the criteria and were radiolabeled with ³H. [³H]GMC-058 was the only compound with negligible binding in controls, and was further evaluated using tissue microarrays, autoradiography on fresh-frozen brain slices, and in vitro saturation binding assay on brain homogenates. [³H]GMC-058 binding co-localized with α -syn inclusions in Parkinson's disease (PD) and multiple-system atrophy (MSA), with dense A- β plaques in cerebral amyloid angiopathy and AD and with p-tau inclusions in progressive supranuclear palsy (PSP) and corticobasal degeneration (CBD). Specific binding was highest in PSP and CBD. In vitro K_D was highest in AD (5.4 nM), followed by PSP (41 nM) and CBD (75 nM). The K_D in MSA, PD, and controls was >100 nM. [³H]GMC-058 is a novel radioligand displaying a low affinity for aggregated α -syn in tissue, with an in vitro profile also suitable for detecting tau pathology in 4R tauopathies.

Keywords: in vitro assay; neurodegeneration; proteinopathy; Lewy bodies

1. Introduction

The accumulation of intracellular aggregates of misfolded α -synuclein (α -syn) is a pathological hallmark of neurodegenerative disorders called synucleinopathies [1]. Such disorders include Parkinson's disease (PD) and dementia with Lewy bodies (DLB), characterized by the accumulation of pathological α -syn in neurons, in the form of Lewy bodies and Lewy neurites [2], and multiple-system atrophy (MSA), characterized by the accumulation of pathological α -syn in glial cells, in the form of glial cytoplasmic inclusions [3].

In the last decade, extensive research and efforts have been devoted to the search and discovery of imaging agents able to detect in vivo pathological α -syn in patients with synucleinopathies using positron emission tomography (PET). Recent clinical studies with newly developed PET tracers [^{18}F]ACI-12589 [4], [^{18}F]SPAL-T-06 [5], and [^{18}F]C05-05 [6] have shown promising results in patients with MSA ([^{18}F]ACI-12589 and [^{18}F]SPAL-T-06) and in patients with Lewy-body disease ([^{18}F]C05-05). However, these PET radioligands present some shortcomings (Table 1).

Table 1. Main in vitro and in vivo characteristics of α -syn PET radioligands evaluated in patients with synucleinopathies.

Radioligand	IC ₅₀ or K _D			Synucleinopathies Evaluated **
	α -syn	A β	pTau	
[^{18}F]ACI-12589	33.5 \pm 17.4 nM (sporadic PD); 28 nM (MSA)	317 nM (AD)		PD ***, MSA (+), DLB
[^{18}F]SPAL-T-06	2.5 nM (MSA)	Not reported		MSA (+)
[^{18}F]C05-05	IC ₅₀ *: 1.5 nM (DLB);	IC ₅₀ * in AD tissue: 12.9 nM		PD/DLB (+) and MSA (+)

* = only 50% of the total binding was displaced in homologous competition experiments. ** = (+) indicates the cases in which specific binding higher than controls was measured. *** = two participants with duplications of the SNCA gene were included in the study.

[^{18}F]ACI-12589 displays in vitro selectivity for α -syn vs. tau and A β , and a K_D in PD and MSA tissue ~30 nM. [^{18}F]ACI-12589 is able to successfully image α -syn pathology only in MSA, likely because the B_{max}/K_D of the radioligand is not adequate enough to detect a lower level of pathology in PD. In the case of [^{18}F]SPAL-T-06 and [^{18}F]C05-05, an IC₅₀ = 2–3 nM in brain homogenates from DLB or MSA cases has been reported using homologous competition binding studies. However, both radioligands have been developed from the same scaffold as PBB3 and also display an affinity to A β and tau. Given that concomitant A β and tau pathology is frequent in Lewy-body disease, particularly DLB and PD with dementia, selectivity for α -syn over A β and tau is a requirement for a fit-for-purpose α -syn PET radioligand. All clinical PET radioligands developed so far lack the properties of combined high B_{max}/K_D and selectivity for α -syn, required to image α -syn pathology in Lewy-body disease with high specificity.

Therefore, a selective PET radioligand able to image α -syn in all synucleinopathies is still a clinically unmet need. The aim of this study was to discover small molecules displaying suitable in vitro profiles (affinity in nM range and >10-fold selectivity for α -syn vs. A β and tau) for development as α -syn PET radioligands. The work included in vitro screening using recombinant α -syn fibrils and brain homogenates from Alzheimer's disease (AD) donors. Compounds with suitable in vitro affinity profiles were radiolabeled with ^3H . Potential candidates were evaluated with in vitro autoradiography (ARG). Brain tissue from control donors and from patients with different proteinopathies was used for ARG

experiments using fresh-frozen tissue sections and paraffine-embedded tissue microarrays (TMAs). High-resolution ARG and immunohistochemistry on consecutive TMA sections were performed to study the co-localization of an ARG signal with α -syn, p-tau and A β pathology.

2. Materials and Methods

2.1. *In Vitro* Binding Assays

2.1.1. Radioligand Binding to α -Syn Fibrils

Compound affinity for α -syn fibrils was measured by means of radioligand binding displacement experiments of an AbbVie tool radioligand with high affinity for α -syn fibrils ($[^3\text{H}]\text{-}\alpha\text{-syn-tool}$). The aggregation of α -syn monomers into fibrils was obtained as described by Bousset et al. [7]. In brief, monomers (5 mg/mL, prepared in AbbVie (Worcester, MA, USA) were incubated in 150 mM of KCl and 50 mM of Tris-HCl (pH 7.5) for 7 days at 37 °C, under constant shaking conditions (650 rpm, Eppendorf Thermomixer C, Eppendorf, Hamburg, Germany). After incubation, the fibrils were harvested via ultracentrifugation (40,100 \times g, 30 min, 20 °C), resuspended in buffer, sonicated (40% amplitude, 10 s pulse on, 5 s pulse off) for 4.5 min at 20 °C, divided into aliquots (5.5 mg/mL), and stored at -80 °C until the day of the experiment. The characterization of the fibrils included protein content determination (BCA method) and an analysis of Proteinase K degradation pattern [7].

On the day of the experiment, α -syn fibrils were thawed for a few minutes at 37 °C, diluted in Dulbecco's Phosphate Buffered Saline (PBS) without calcium and magnesium, pH = 7.4 (DPBS) plus 0.1% bovine serum albumin (BSA), and incubated (at the final fibrils concentration of 2.5 $\mu\text{g/mL}$) for 60 min, at room temperature (RT), with 5 nM $[^3\text{H}]\text{-}\alpha\text{-syn-tool}$, in the absence or presence of different concentrations of non-radiolabeled compounds. Bound radioligand was separated from free radioligand via rapid filtration and washings with cold DPBS, using a Unifilter-96 GF/B filter plate (PerkinElmer, Rodgau, Germany) presoaked in 0.3% polyethylenimine (PEI) and a Unifilter Cell Harvester (PerkinElmer, Rodgau, Germany). Plates were air-dried, and the scintillation liquid (Betaplate Scint, PerkinElmer) was added and counted using a MicroBeta2 2450 (PerkinElmer, Rodgau, Germany). Non-specific binding (NSB) was defined as the binding in the presence of 10 μM unlabeled α -syn tool. Data fitting and the constant of inhibition (K_i) calculation was performed using the software platform from Dotmatics (Boston, MA, USA).

2.1.2. Radioligand Binding to Native Tau and A β Fibrils

Compounds' affinity for tau and A β fibrils was measured by means of radioligand binding displacement experiments on AD brain homogenates, using $[^3\text{H}]\text{NFT-355}$ [8] (AbbVie, North Chicago, IL, USA) and $[^3\text{H}]\text{Pittsburg Compound-B (PiB)}$ (Novandi Chemistry AB, Södertälje, Sweden [9]) to label tau and A β aggregates, respectively. Flash-frozen tissue from the frontal cerebral cortex of an AD (Braak stage V) brain was purchased from Analytical Biological Services Inc. (ABS; Wilmington, DE, USA), homogenized in DPBS, divided into aliquots (10 mg/mL), and stored at -80 °C until the day of the experiment.

On the day of the experiment, the brain homogenate was brought to RT, diluted in DPBS plus 0.1% BSA and incubated for 90 min, at RT, with 0.5 nM $[^3\text{H}]\text{NFT-355}$ or 1 nM $[^3\text{H}]\text{PiB}$, in the absence or presence of different concentrations of non-radiolabeled compounds. Bound radioligand was separated from free radioligand via rapid filtration and washings with cold DPBS, using a Unifilter-96 GF/B filter plate (presoaked in 0.3% PEI) and a Unifilter Cell Harvester (PerkinElmer). Plates were air-dried, and the scintillation liquid (Betaplate Scint, PerkinElmer) was added and counted using a MicroBeta2 2450.

NSB was defined as the binding in the presence of 10 μM T808 [10] (AbbVie Germany) and 10 μM PiB for [^3H]NFT-355 and [^3H]PiB, respectively. Data fitting was performed using the software platform from Dotmatics (Boston, MA, USA).

2.2. Radiosynthesis of [^3H]GMC-058, [^3H]GMC-073, and [^3H]GMC-098

Chemicals and solvents were obtained from commercial sources and were used without further purification. NMR spectra were recorded on a Bruker 500 MHz AVANCE III system using standard Bruker pulse sequences. Experiments were run in D6-DMSO at 25 °C. ^1H NMR chemical shifts were referenced relative to the residual solvent peak at 2.50 ppm, and ^{13}C NMR chemical shifts were referenced to 39.5 for D6-DMSO. Flash column chromatography was carried out using prepacked silica gel columns supplied by Biotage and using a Biotage automated flash system with UV detection. Preparative HPLC was performed using a Waters Xbridge C18 5 μ OBD 19X150 mm, 25 mL/min, 30% for 2 min and then was ramped to 95% over 18 min and held for 3 min MeCN-0.2% aq. NH_4OH was used unless otherwise indicated. Reactions with tritium gas were performed on an RC Tritec tritium manifold. Analytical HPLC was carried out using an Agilent 1100 series HPLC using a Waters 4.6 \times 100 mm Xbridge C18 3.5 μ , with the following elution profile: 5% for 3 min and then ramped to 95% over 22 min and hold 95% for 5 min MeCN/water 10 mM NH_4HCO_3 pH 10 with radioactive detection using a LabLogic Beta-Ram 4 detector. LCMS analysis was carried out using a Waters 1100 HPLC system with a Waters 3100 mass detector on an XSelect CSH C-18 4.6/150 mm, 3.5 μm with a gradient of 5–100% MeCN–0.1% formic acid (adjusted to pH 3) over 10 min followed by a 2 min wash with 100% MeCN or on a Waters1200 series UPLC with a Waters 4.6 \times 100 mm Xselect CSH C18 3.5 μ , 5 to 95% MeCN/water 0.2% formic acid pH 3 for 1.85 min then isocratic elution for 0.1 min with mass detection using a QDA mass detector. The molar activities of the products were determined via LC/MS using Isopat2 to deconvolute the MS signals [11]. Liquid scintillation counting was performed with a Beckman LS 6500 scintillation counter.

2.3. Autopsy Material

Frozen human brain tissues from patients with Parkinson's disease (PD), Lewy-body disease (LBD), multiple-system atrophy (MSA), corticobasal degeneration (CBD), and non-dementia controls were obtained from the Netherlands brain bank (Table 2) and frozen human tissues from patients with MSA, PSP, and one control were obtained from the UK brain bank (Table 3). Formalin-fixed paraffine-embedded tissue blocks from patients with different synucleinopathies were obtained from the Netherland Brain Bank (Table A1). Approval for the use of the autopsy material for the project was obtained from the Swedish Ethical Research Authority. Brain homogenates were obtained from tissue of AD, CBD, PSP, MSA-P patients, and healthy controls, obtained from the Alzheimer's Disease Research Center of the University of Pittsburgh (Table A2), from the University of California San Francisco (Table A3), and from the Banner Sun Health Research Institute (Table A4).

Table 2. Demographic data of cases from the Netherlands Brain Bank selected for autoradiography studies using fresh-frozen tissue.

Case n.	Diagnosis	Age	Sex	PMI (h)	Brain Region
PD1	Parkinson's disease	69	M	7	Cingulate gyrus
PD2	Parkinson's disease	77	M	5	Cingulate gyrus
PD3	Parkinson's disease	75	M	6	Cingulate gyrus
LBV1	Lewy-bodies variant	83	M	5	Cingulate gyrus
LBV2	Lewy-bodies variant	54	M	5	Cingulate gyrus
MSA1	Multi-system atrophy	66	M	5	Cerebellum
MSA2	Multi-system atrophy	69	F	5	Cerebellum
CBD1	Corticobasal degeneration	58	F	7	Superior frontal gyrus
C01	Non-dementia control	81	F	4	Cingulate gyrus
C02	Non-dementia control	51	M	8	Cingulate gyrus
C03	Non-dementia control	79	F	11	Cingulate gyrus

Table 3. Demographic data of cases from the UK Brain Bank selected for autoradiography studies using fresh-frozen tissue.

Case n.	Diagnosis	Age	Sex	PMI (h)	Brain Region
MSA3	Multiple-system atrophy	58	F	10	Cerebellum
MSA4	Multiple-system atrophy—cerebellar form	52	M	33	Cerebellum
PSP1	Progressive supranuclear palsy	66	M	8	Globus pallidus
PSP2	Progressive supranuclear palsy	77	F	11	Globus pallidus
C04	Control	68	M	7.5	Caudate, putamen and globus pallidus

2.4. Preparation of Human Brain Tissue for In Vitro Binding Studies

As described in Bagchi et al. [12], to prepare insoluble fractions from PD and MSA-P patients, fresh-frozen tissue blocks were sequentially homogenized in four buffers (3 mL/g wet weight of tissue) with glass Dounce tissue grinders (Kimble, Vineland, NJ, USA): (1) high salt (HS) buffer: 50 mM Tris-HCl pH 7.5, 750 mM NaCl, 5mM EDTA; (2) HS buffer with 1% Triton X-100; (3) HS buffer with 1% Triton X-100 and 1M sucrose; and (4) phosphate-buffered saline (PBS). Homogenates were centrifuged at $100,000 \times g$ after each homogenization step, and the pellet was resuspended and homogenized in the next buffer in the sequence. For AD, CBD, PSP, and CT cases, the frozen tissue blocks were prepared as described by Stehouwer et al. [13]. In brief, tissue blocks were thawed and homogenized in ice-cold pH 7.0 phosphate-buffered saline (PBS) at 300 mg/mL on ice using a glass homogenizer, diluted 30-fold with PBS to 10 mg/mL, and homogenized a second time with a Brinkmann Polytron homogenizer before storage at -80°C .

2.5. Saturation Binding Assays

Saturation binding assays were performed in AD, CBD, PSP, MSA-P, PD, and healthy patients brain homogenates (0.1 mg/mL tissue) using a [^3H]GMC-058 concentration range of 0.9 nM to 80 nM and incubation for 90 min at room temperature (RT) with PBS + 20% EtOH. Non-specific binding was determined using 10 μM of unlabeled GMC-044. After incubation, samples were filtered under vacuum on equilibrated GF/B UniFilter plates (PerkinElmer) using the FilterMate 196 (PerkinElmer). Afterwards, filters were washed three times with 250 μL chilled buffer (PBS + 20% EtOH). [^3H]GMC-058 binding was measured with a beta scintillation counter (PerkinElmer). The saturation data was fitted and analyzed using the non-linear regression function of GraphPad Prism 10 software

to calculate the dissociation constant (K_D) and maximum number of binding sites (B_{max}). Scatchard plots were prepared with GraphPad Prism 10 software to display the saturation binding data.

2.6. Autoradiography Experiments on Fresh-Frozen Tissue Sections

Selections of frozen human sections (described in Tables 2 and 3) were used for binding autoradiography. Sections were first pre-incubated for 20 min in binding buffer [50 mM Tris-HCl (pH 7.4), 120 mM NaCl, 5 mM KCl, 2 mM CaCl₂, 1 mM MgCl₂, and 0.1% BSA] and then incubated with [³H]GMC-058 (specific activity 22 Ci/mmol); [³H]GMC-073 (specific activity 23.4 Ci/mmol); or [³H]GMC-073 (specific activity 26.4 Ci/mmol) in binding buffer for 180 min at RT. In the pilot autoradiography experiment (Figure A1). [³H]GMC-058 was tested at 25 and 50 nM, while [³H]GMC-073 and [³H]GMC-098 were each tested at 10 and 20 nM. For all other autoradiography in fresh-frozen tissue sections, 25 nM [³H]GMC-058 was used. To determine NSB, adjacent brain sections were incubated with [³H]-tracer mixed with 5 μM of unlabeled GMC-044. The binding reaction was stopped with two 10 min washes in washing buffer [50 mM Tris-HCl (pH 7.4) at 4 °C] and a brief dip in cold distilled water. Slides were allowed to air-dry before being placed under storage phosphor screens (Fujifilm Plate BAS-TR2025, Fujifilm, Tokyo, Japan) in imaging cassettes for 90 h together with ART0123C and ART0123B tritium standards on glass slides (American Radiolabeled Chemicals Inc., St. Louis, MO, USA). Storage phosphor screens were scanned using an Amersham Typhoon FLA-9500 phosphor imaging scanner (Cytiva, Marlborough, MA, USA), and the resulting images were analyzed using Multi Gauge 3.2 phosphor imager software (Fujifilm, Tokyo, Japan) for ROI delimitation, density calibration, and quantification. Quantitative binding data from duplicates of the total, and NSB were plotted and analyzed using graphPad Prism v10 (GraphPad Software, Boston, MA, USA). Specific binding was determined by subtracting the non-specific signal from the total signal. The toluidine blue staining of adjacent sections was used to obtain anatomical references for white- and gray-matter ROI selection. Care was taken not to include artifact signals in the ROIs analyzed. These artifacts were identified as randomly placed punctate signals appearing in both total and NSB images, and they often coincided with small folds or tears in the tissue sections.

2.7. Autoradiography and Emulsion Autoradiography on Tissue Microarrays

Tissue micro-arrays (TMAs), prepared from paraffin-embedded tissue from human post-mortem tissue as described in [14], were first de-paraffinized with two 1 h and one overnight incubation in Neo-Clear Xylene Substitute (Sigma-Aldrich, St. Louis, MO, USA) at 37 °C and then dehydrated in three short incubations at RT with decreasing concentrations of ethanol before autoradiography with [³H]GMC-058 was performed as described above. For the saturation binding autoradiography, duplicate slides of each TMA set were incubated with 0.3 nM to 200 nM [³H]GMC-058. Adjacent sections were co-incubated with 5 μM of unlabeled GMC-044 to calculate NSB. The quantification of total and non-specific binding was performed via delineation of the ROIs on the whole core, except for MSA, where the ROI followed the areas in which the binding of [³H]GMC-058 corresponded to areas with α-syn inclusions. Those cores that had imperfections or were incomplete were not included in the analysis, or only the area of remaining tissue that adhered to the glass slide was delineated. For the cores from the substantia nigra of PD patient cases, the cores selected for analysis were those containing α-syn inclusion, but no A-β deposits or pTau tangles. The information was collected from IHC analysis of adjacent TMA slides.

For high-resolution emulsion autoradiography, an autoradiography experiment with TMAs using 25 nM [^3H]GMC-058 was performed as described above. At the end of the 90 h exposure to the storage phosphor screen, slides were stored in a vacuum until dipping in a photoemulsion. In the dark, using a sodium lamp, Agar Scientific, AGP9284 type NTB emulsion was melted in a heated water bath and diluted (1:1) with ddH₂O. The emulsion was poured into dipping chambers, and the slides were dipped and placed vertically to air-dry. When completely dry, the slides were placed in a light-tight slide box with desiccant and exposed at 4 °C for 1–12 weeks. After exposure, the slides were developed in diluted Phenisol Developer for 2 min, rinsed in water, and fixed in hypam Fixer at 17 °C in a water bath. After rinsing in water, the slides were counterstained with Harris HTX, dehydrated in graded ethanol, cleared in Xylene, and mounted in Pertex. Images were taken using a 3D Histech P250 III scanner (3DHISTECH Kft. Hungary) at up to 15 focal layers with a distance of 0.2 μm .

2.8. Immunohistochemistry

Immunohistochemical chromogenic (IHC) staining was made essentially as in [15], and the reference antibodies for the respective proteinopathies used were Signet laboratories (Abeta 6E10, Abeta 4G8), Abcam (Anti-Alpha-synuclein antibody [LB 509]), and Thermo Fisher Scientific (Waltham, MA, USA) (AT-8 Phospho-PHF-Tau). Briefly, 5 μm slide-mounted tissue sections were performed according to a standardized protocol with modifications to optimize the specificity of the observed staining patterns. IHC staining was performed using the Discovery Ultra platform (Ventana, Roche Diagnostics International AG, Rotkreuz, Switzerland) automated immunostaining robot, using the OmniMap DAB chromogenic staining kit (Ventana Medical Systems) according to the manufacturer's instructions. In brief, initial deparaffinization, followed by heat-activated antigen retrieval in a pH 8.0 buffer for 92 min (Ventana Medical Systems' (Ventana) DISCOVERY CC1 (DISCOVERY Cell Conditioning Solution 1, 06414575001, 950–500), was performed to improve the detection of antigens in the FFPE tissue. Endogenous tissue peroxidases (Inhibitor CM, Ventana), which may interfere with the assays, were blocked with 0.3% hydrogen peroxide. The primary antibody for phosphorylated Tau detection (AT-8 pTau [In vitrogen, MN1020] at 2 $\mu\text{g}/\text{mL}$), and re for total Abeta (Mouse anti-Abeta 4G8 [Signet, Covance, 800709 (SIG-39200)], were mixed and co-incubated at a final concentration of 1 $\mu\text{g}/\text{mL}$ and applied on the tissue sections. For the IHC staining of α -synuclein inclusions, the anti-human α -synuclein antibody LB509 (Abcam, GR300971) 0,5 $\mu\text{g}/\text{mL}$ was used. Prior to staining, sections were treated for 24 min with protease (Ventanas Protease 1, [760–2018]) to degrade soluble α -synuclein species. Antibodies were followed by incubation with the HRP-conjugated secondary antibody (the HRP labeled OmniMap goat anti-Mouse Ab, 05269652001 760–4310), and the visualization of the positively stained cells was performed through the addition of hydrogen peroxide and DAB (DISCOVERY ChromoMap DAB Kit [Ventana, 760–159] (single IHC)], resulting in an insoluble brown (DAB) staining precipitate at the site of antibody binding. Counterstaining for IHC was performed with hematoxylin [Hematoxylin II, Ventana, 760–2208 and Bluing Reagent, Ventana, 760–2037]. The stained slides were subsequently scanned at up to 10 focal layers in brightfield (20 \times –40 objective) using a digital whole slide scanner (Pannoramic 250 III Scanner, 3DHistech, Budapest, Hungary). Analysis was performed of the IHC stained tissue sections via manual evaluation using a digital image viewer software (CaseViewer_2.0_RTM_v2.0.2.61392). All analyses of the stained and labeled tissue sections with reference antibodies for A β , p-tau, and α -syn and/or ligands were compared, side by side, to each other. Adjacent fresh-frozen tissue sections or TMAs were used when comparing IHC immunoreactivity with an autoradiography binding signal.

3. Results

The work plan for this study included a first part that was devoted to the discovery of small molecules with an *in vitro* profile suitable for the development of a selective α -syn ligand and a second part that included the *in vitro* characterization of lead candidates.

The discovery part included compound design and *in vitro* competition experiments for the identification of lead candidates. The *in vitro* characterization included ^3H -radiolabeling, *in vitro* saturation binding, and autoradiography experiments in tissues from donors with different proteinopathies.

3.1. Discovery and *In Vitro* Characterization of GMC-058

3.1.1. Discovery of GMC-058, GMC-073 and GMC-098

A library of 78 small molecules was generated based on available information from the public domain. Four optimization cycles were performed with radioligand binding assays to measure the affinity of compounds for *in vitro*-assembled α -syn fibrils and native tau and A β fibrils in AD homogenates.

Sixteen of these compounds showed affinity for α -syn fibrils < 30 nM and for A β and tau > 50 nM (Table A5). The criteria for selection were K_i for α -syn < 30 nM and K_i for tau and A β > 200 nM.

Three compounds, GMC-058, GMC-073, and GMC-098, were selected based on those criteria and on the feasibility of radiolabeling. The K_i of GMC-058, GMC-073, and GMC-098 using recombinant α -synuclein fibrils was 22.5 nM, 8 nM, and 9.7 nM, respectively.

All three compounds showed a lower affinity for A β ($K_i = 1490$ nM for GMC-058, 2630 nM for GMC-073, and 226 nM for GMC-098) and tau ($K_i = 1320$ nM for GMC-058, 248 nM for GMC-073, and 805 nM for GMC-098) in AD brain homogenates. GMC-058 (Figure 1), GMC-073, and GMC-098 were, therefore, selected for radiolabeling with ^3H .

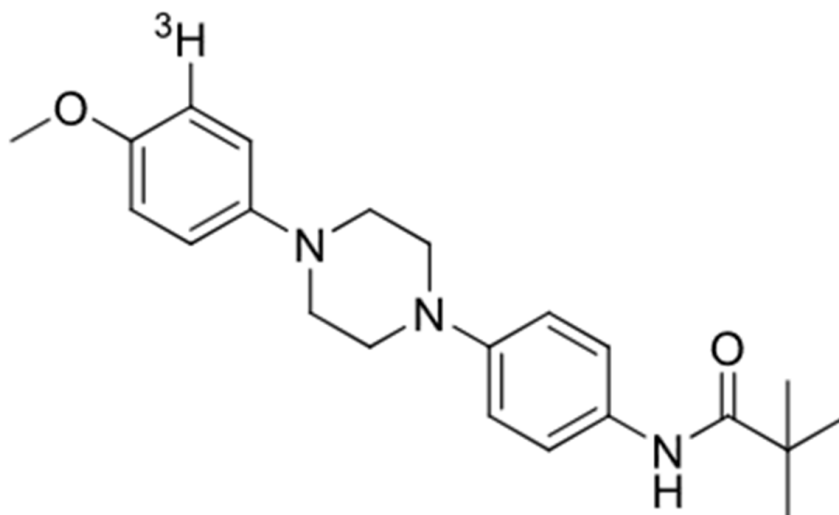


Figure 1. Chemical structure of [^3H]GMC-058.

3.1.2. Autoradiography Experiments with [^3H]GMC-058, [^3H]GMC-073 and [^3H]GMC-098

The three [^3H]-labeled compounds were initially evaluated through autoradiography in tissue sections from the cingulate cortex of healthy controls.

[^3H]GMC-073 and [^3H]GMC-098 displayed clear binding in control cingulate cortex tissue, approximately 50% of which was displaced via 5 μM GMC-044, whereas [^3H]GMC-058 displayed negligible binding (Figure A1 and Table A6). The nature of this off-target displaceable binding is not known. [^3H]GMC-058 was selected for further evaluation in pathological tissue sections.

3.1.3. In Vitro Saturation Binding Assays with [³H]GMC-058 in Brain Homogenates

Saturation binding assays with [³H]GMC-058 were conducted in brain homogenates from cases with AD, PSP, CBD, MSA-P, PD, and Controls (Figures 2 and A2).

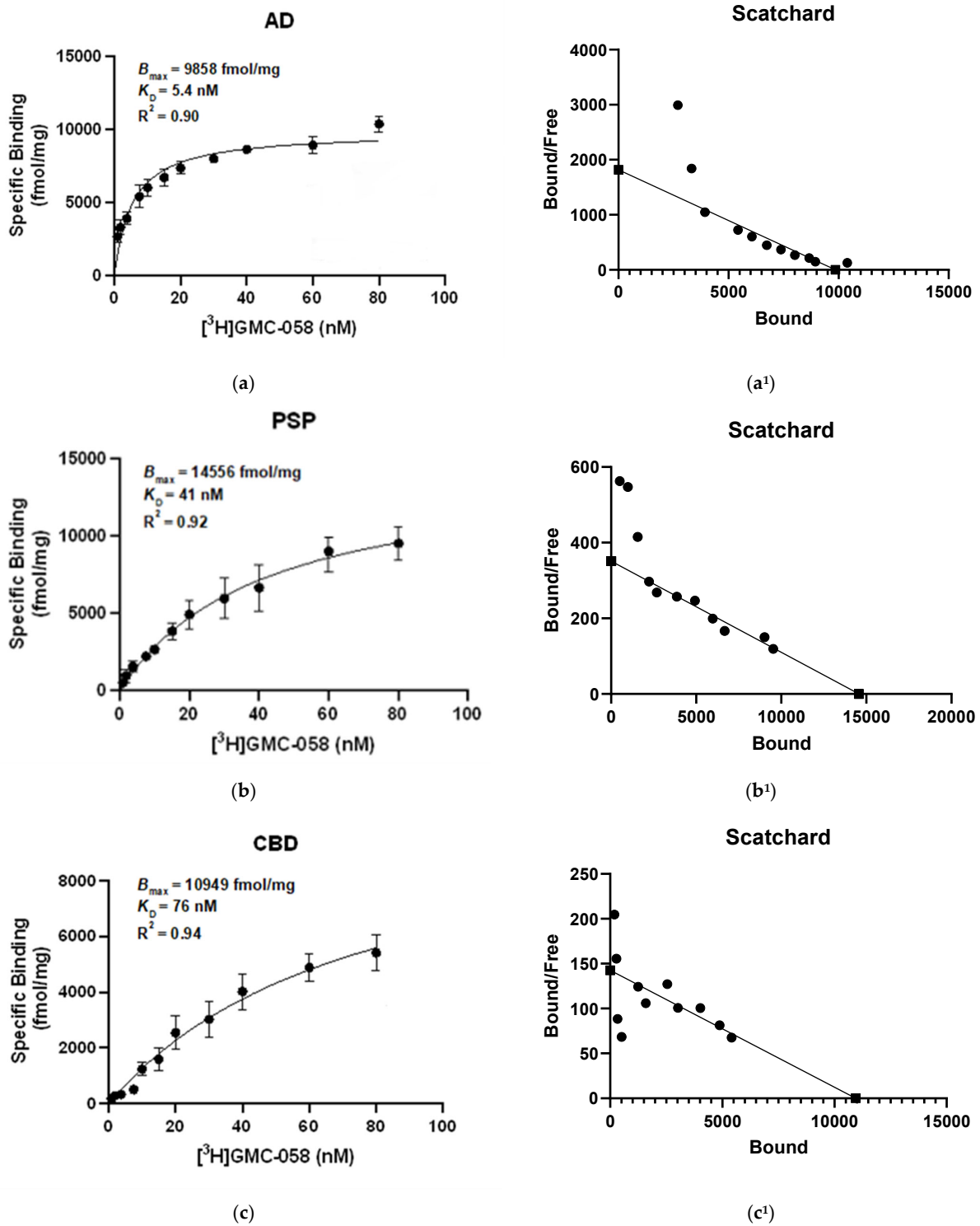


Figure 2. Cont.

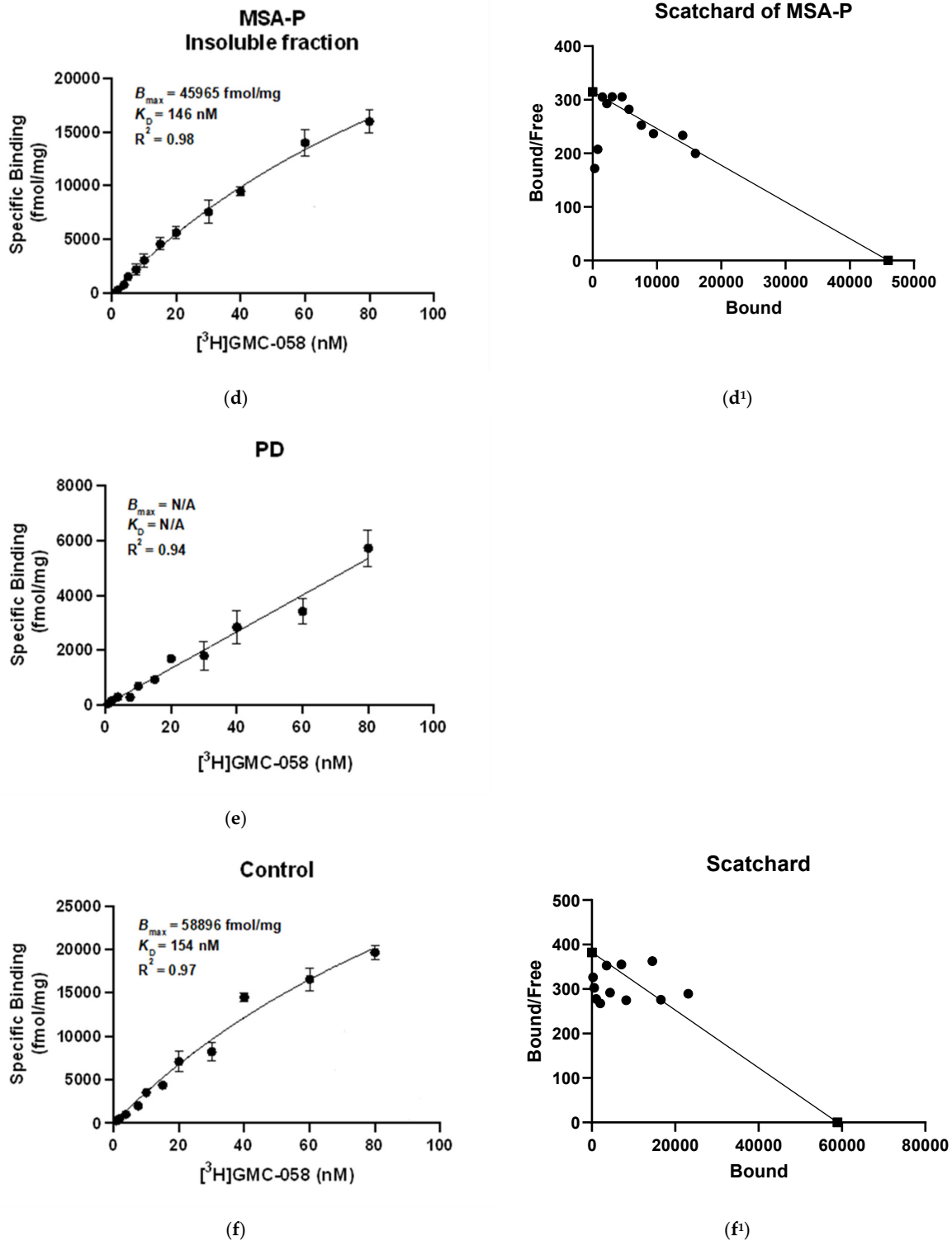


Figure 2. [^3H]GMC-058 saturation binding assays in (a,a¹) AD, (b,b¹) PSP, (c,c¹) CBD, (d,d¹) MSA-P, (e) PD and (f,f¹) control brain homogenates. [^3H]GMC-058 saturation binding assays were carried out in brain tissue homogenates from AD, PSP, CBD, MSA-P, PD, and control cases using concentrations of 0.9 to 80 nM. Non-specific binding was determined using 10 μM of unlabeled GMC-058. Scatchard plots indicating B_{max} and K_D values. Error bars represent the mean \pm SD for two experiments in triplicates. B_{max} = maximum number of binding sites; K_D = dissociation constant.

The K_D estimated in AD tissue was 5.4 nM, and in PSP tissue, it was 46 nM, while in CBD tissue, it was 71 nM. In brain homogenates from MSA-P and control cases, the K_D was >100 nM. No evidence of saturation binding was observed in PD tissue.

3.1.4. Autoradiography Experiments with [³H]GMC-058

Autoradiography experiments using 25 nM [³H]GMC-058 in tissue sections from the cingulate cortex of controls and PD patients and from the cerebellum of MSA patients did not show clear evidence of specific binding higher than the displaceable (off-target) binding in controls (Figures 3 and A3 and Table A7). Saturation [³H]GMC-058 binding autoradiography experiments in TMAs showed that specific binding did not reach saturation in any of the tissues (Figures A4 and A5) and did not permit us to obtain reliable K_D estimates.

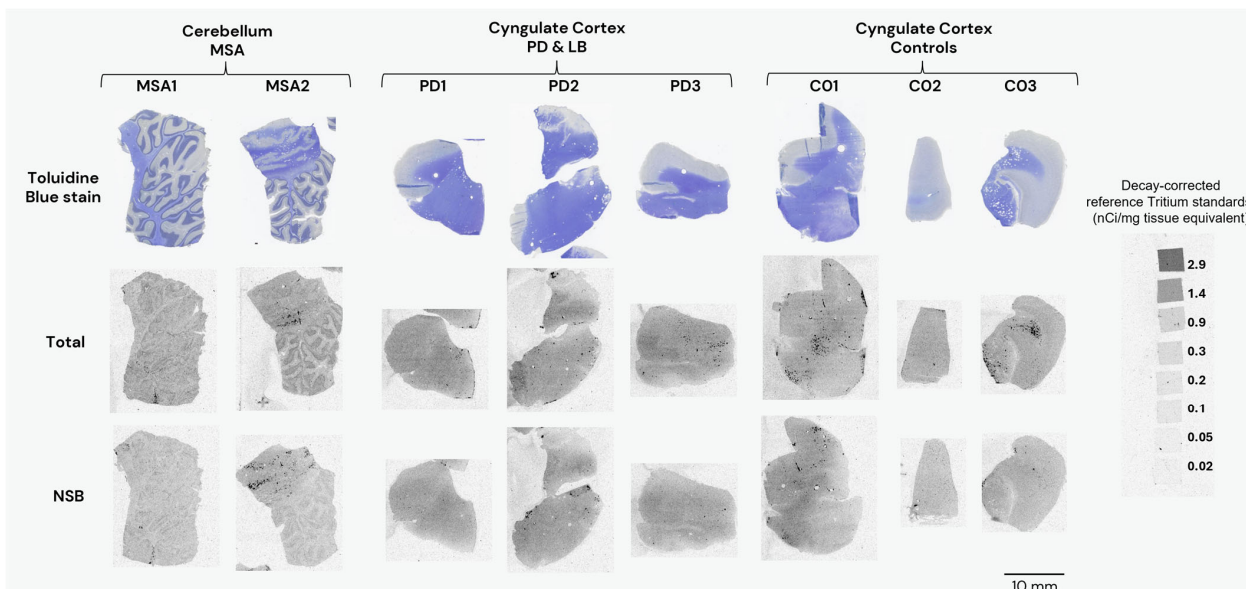


Figure 3. Representative images from autoradiography with [³H]GMC-058 (25 nM) on fresh-frozen tissue sections from patients with multiple-system atrophy (MSA), Parkinson’s disease (PD), Lewy-body disease (LB), and controls. Non-specific binding was measured with excess (5 μM) of blocker (GMC-044). Line scale: 10 mm.

However, the specific binding data obtained at the concentration of 25 nM [³H]GMC-058 showed clear differences in specific binding and were thus selected for group comparison.

In synucleinopathies (PD and MSA), cerebral amyloid angiopathy (CAA), AD, and 4R tauopathies (PSP and CBD), the specific binding of 25 nM [³H]GMC-058 was significantly higher than the displaceable binding in controls ($p < 0.01$, ANOVA with Dunnett’s multiple comparisons test; see Table 4 and Figure A6). High-resolution autoradiography showed that the binding of 25 nM [³H]GMC-058 co-localized with α-syn inclusions in PD and MSA, with dense Aβ plaques in CAA and AD, and with p-tau inclusions in PSP and CBD (Figures 4 and A7–A9).

Table 4. Specific binding (fmol/mg tissue equivalent) of 25 nM [³H]GMC-058, measured in TMAs from cases with different proteinopathies. In non-dementia controls (NDE) and liver tissue, the values refer to displaceable (off-target) binding.

TMA	NDE	Liver Control	MSA	CAA	AD	CBD	PSP	PD
N=	8	4	1	3	4	2	2	6
Mean (±SEM)	70 (4)	57 (7)	166 ** (19) †	131 ** (12)	127 ** (15)	204 *** (38)	173 *** (2)	129 *** (7)

NDE = non-dementia elderly controls; MSA = multiple-system atrophy; CAA = cerebral amyloid angiopathy; AD = Alzheimer’s disease; CBD = corticobasal degeneration; PSP = progressive supranuclear palsy; PD = Parkinson’s disease. *** $p < 0.0001$; ** $p < 0.01$, compared to NDE control, obtained via one-way ANOVA with Dunnett’s multiple comparisons test. † SEM from 10 technical replicates of $n = 1$ MSA case.

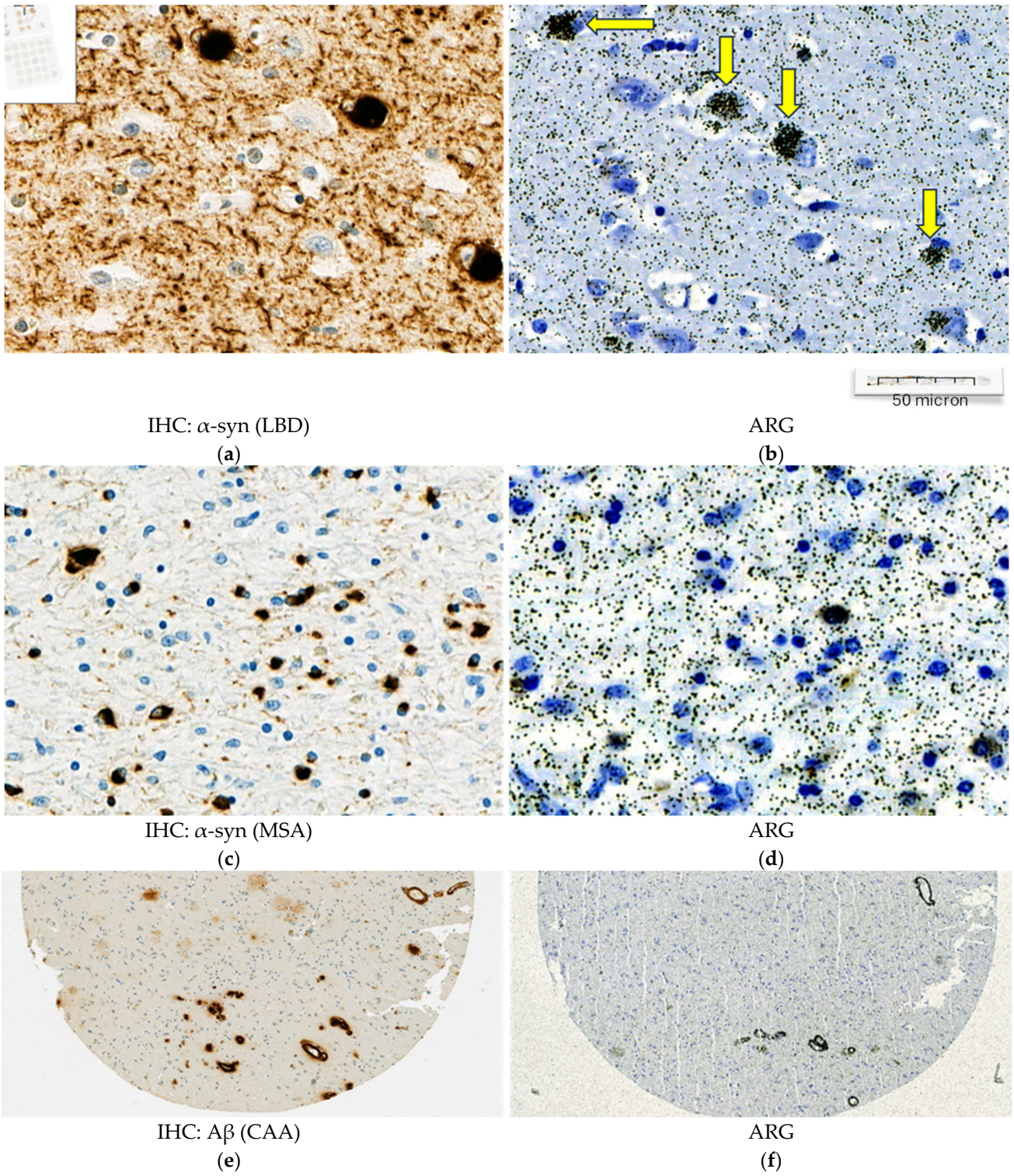


Figure 4. Cont.

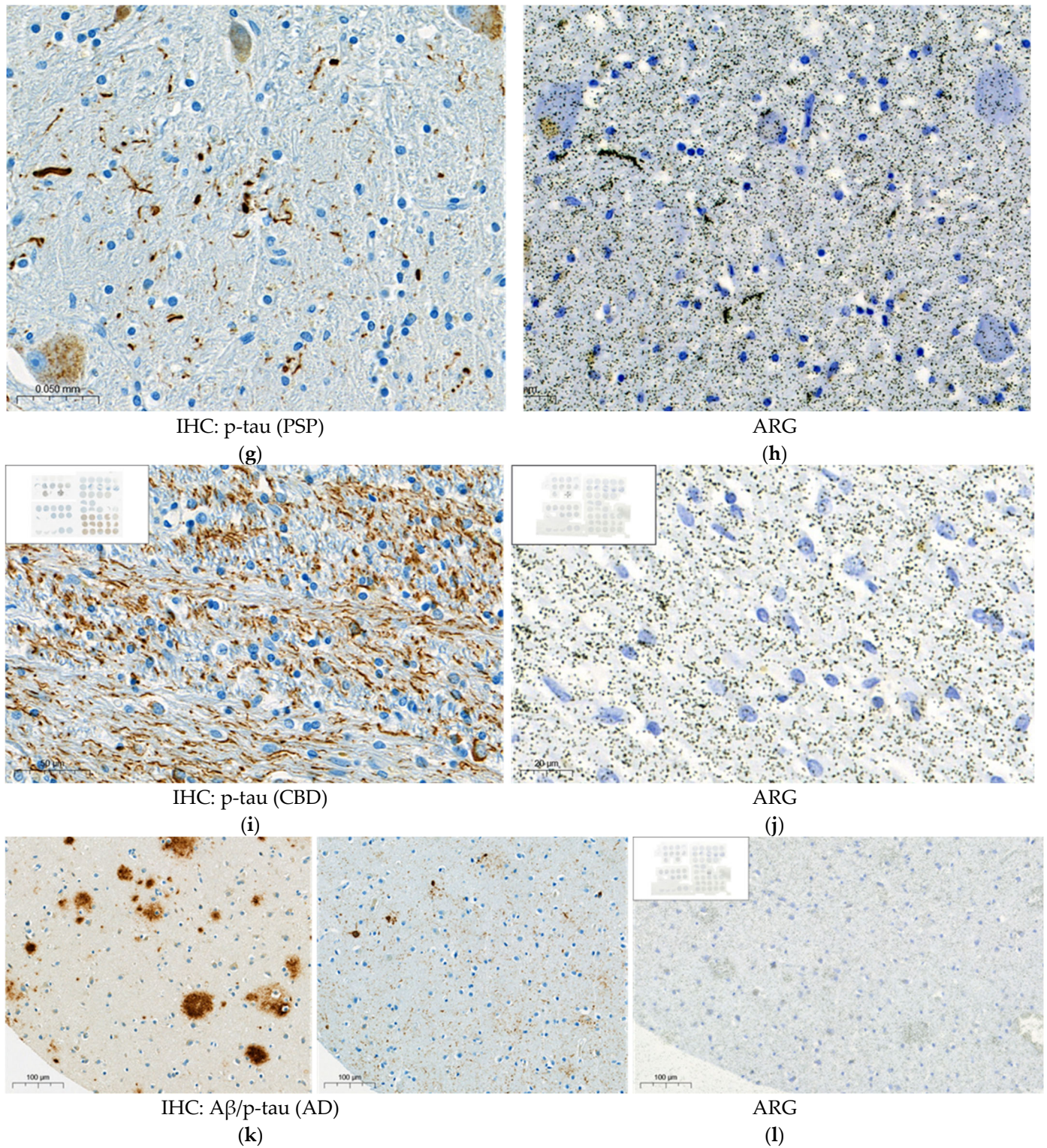


Figure 4. Representative high magnification images from α -synuclein (α -syn), amyloid beta ($A\beta$) and, phospho-tau (p-tau) immunohistochemistry (IHC) and emulsion autoradiography (ARG) with 25 nM [3H]GMC-058. (a–d) In two representative LBD (a,b) and MSA cases (c,d), the ARG signal (yellow arrows) corresponds to Lewy bodies (a) and oligodendrocytic inclusions (c). (e,f) In CAA cases, the ARG signal corresponds to dense perivascular $A\beta$ deposits (e). (g–j) In PSP (g,h) and CBD (j,k), the ARG signal seems to localize in areas of p-tau positive inclusions (g,i). (k,l) In AD the case with abundant $A\beta$ plaques and p-tau inclusions (k), a weak ARG signal was observed (l).

We then conducted autoradiography experiments in fresh-frozen tissue for which α -syn, A β , and p-tau expression was measured via IHC. We selected tissue sections of cerebellum from two donors with MSA, of superior frontal gyrus from one donor with CBD, of globus pallidus (GP) from two donors with PSP, and of the cingulate cortex, caudate, GP, and putamen from two controls (Figures 5 and A10 and Table A8).

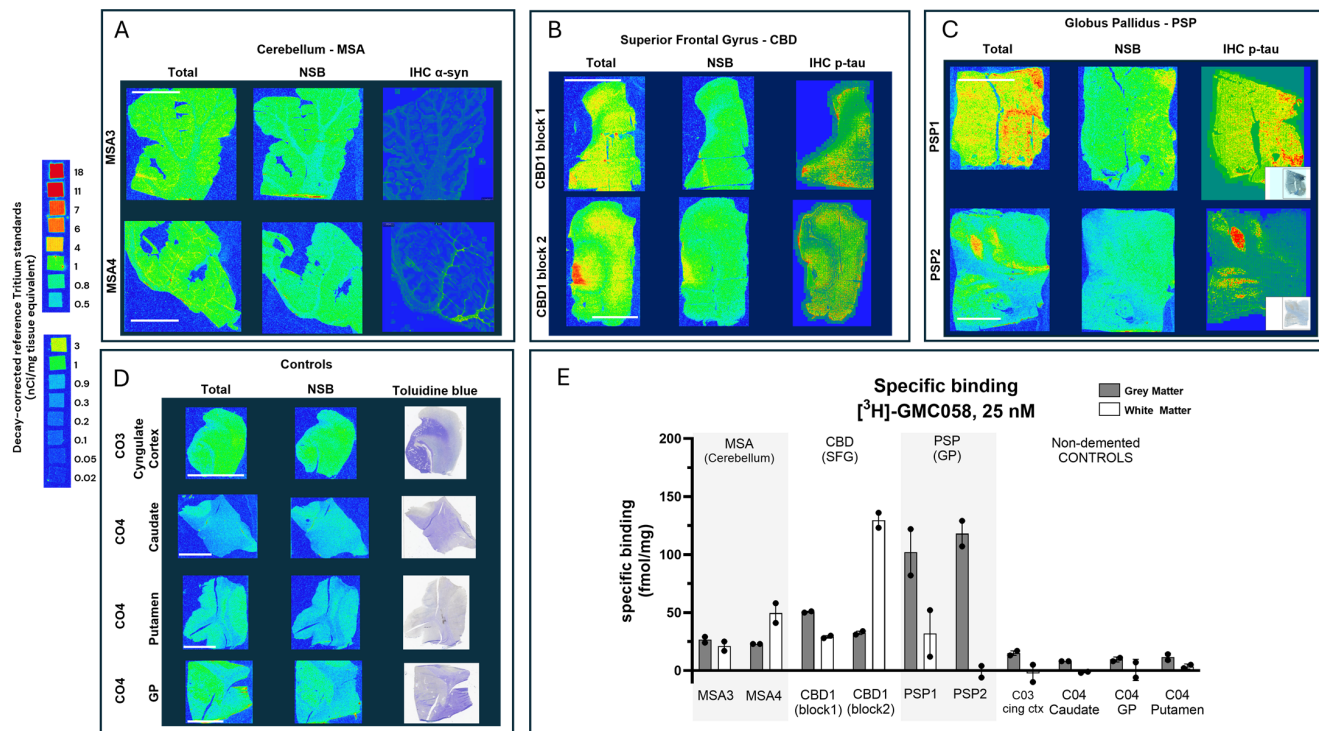


Figure 5. Representative images from autoradiography with [3 H]GMC-058 (25 nM) and corresponding immunohistochemistry (IHC) heatmap showing the density of α -synuclein (α -syn) or phospho-tau (p-tau) immunoreactivity on fresh-frozen tissue sections from patients with (A) multiple-system atrophy (MSA); (B) cortical-basal degeneration (CBD); (C) progressive supranuclear palsy (PSP); and (D) non-dementia controls. Non-specific binding was measured with excess (5 μ M) of cold blocker (GMC-044). (E) Specific binding (fmol/mg) quantified from gray and white matter regions of interest in all cases. Bars represent the average \pm s.e.m. of two technical replicates quantified from each case. Line scale: 10 mm. C04 was negative for pTau, α -Syn, and A β ; therefore a Toluidine blue stain is shown in (D).

In the two MSA cases, specific binding measured in cerebellar gray matter was two-fold higher than the average displaceable binding measured in the gray matter of the cingulate cortex, caudate, the globus pallidus, and the putamen of the controls (Figure 5A,D,E). In CBD and PSP cases, the specific binding in the gray matter of the superior frontal gyrus and the globus pallidus was, on average, three-fold and ten-fold higher, respectively, than the displaceable binding measured in controls (Figure 5B,C,E). No specific binding was observed in the white matter of control cases, whereas in MSA and CBD cases, the average specific binding was 35 to 80 fmol/mg (Figure 5A,B,E and Table A8).

4. Discussion

This study was designed to identify a small molecule with in vitro properties suitable for development as ligand binding to pathological α -syn. We identified three compounds, GMC-058, GMC-073, and GMC-098, that displayed selective binding to recombinant α -syn fibrils. The three compounds were radiolabeled with 3 H, and among the three compounds, [3 H]GMC-058 was selected since it showed the lowest non-displaceable binding in con-

trol tissue. However, when [³H]GMC-058 was further evaluated in human brain tissue homogenates and sections, it displayed low specific binding in synucleinopathy cases but clear specific binding in PSP and CBD cases. This observation was unexpected, considering that the K_i of GMC-058 measured in recombinant α -syn fibrils was 22.5 nM, and in tau-enriched AD tissue was >200 nM. It is possible that the affinity of GMC-058 measured using recombinant α -syn fibrils was different from the affinity of [³H]GMC-058 to native α -syn fibrils in tissue slices or brain homogenates, resulting in a discrepancy between the two different assay results. With regards to tau, since the competition studies were performed using the reference tau tracer [³H]NF-355, it is possible that GMC-058 recognizes a different binding site on tau fibrils. Several radioligands have been developed for imaging tau pathology [16]. Second-generation tau PET radioligands [¹⁸F]PI-2620 and [¹⁸F]PM-PPB3 (also known as [¹⁸F]APN-1607, or florzolotau) have been studied in patients with AD [17,18] and PSP [19,20]. Those studies showed that both radioligands can image 3R and 4R tau pathology in vivo. More recently, the discovery, in vitro characterization, and in vivo pre-clinical assessment of [¹⁸F]OXD-2314 has been reported [21], indicating that this radioligand also has the potential to image 3R and 4R tauopathies. Although [³H]GMC-058 has been designed and developed as a potential α -syn PET radioligand, the in vitro properties suggest that the B_{max}/K_D is not high enough to enable imaging of α -syn pathology in vivo. On the other hand, the evidence of higher specific binding of [³H]GMC-058 in PSP and CBD than in MSA, suggests that GMC-058 might have potential as a PET radioligand for imaging 4R tauopathies. A discrepancy was observed between the high K_D (>50 nM) of [³H]GMC-058 in brain homogenates from PSP and CBD cases and the clear evidence of specific binding in fresh-frozen brain sections from CBD and PSP cases. A similar discrepancy between the results of in vitro saturation studies in brain homogenates and autoradiography studies on brain sections has been observed for another potential α -syn tracer, [³H]-4i, and is difficult to explain [22].

5. Conclusions

[³H]GMC-058 is a novel radioligand displaying a low in vitro affinity for aggregated α -syn, with an in vitro profile also suitable for imaging tau pathology in 4R tauopathies. Further evaluations, including radiolabeling with ¹¹C and in vivo imaging in non-human primates, are warranted to further assess the potential of GMC-058 as a potential PET radioligand for 4R tau.

Author Contributions: Conceptualization, A.V., S.J.F. and M.S.; methodology, V.C.S., M.M., S.B., G.N., L.K., I.G., C.S.E., D.S. and D.S.G.; formal analysis, V.C.S., M.M., S.B., D.S. and D.S.G.; investigation, A.V., V.C.S., M.M., S.B., G.N., L.K., I.G., C.S.E., D.S., D.S.G., S.J.F. and M.S.; resources, A.V., V.C.S., M.M., S.B., G.N., C.S.E., D.S., D.S.G., S.J.F. and M.S.; data curation, A.V., V.C.S., M.M., S.B., G.N., C.S.E., D.S., D.S.G., S.J.F. and M.S.; writing—original draft preparation, A.V.; writing—review and editing, A.V., V.C.S., M.M., G.N., L.K., I.G., C.S.E., D.S., D.S.G., S.J.F. and M.S.; visualization, A.V., V.C.S., M.M., D.S., D.S.G. and M.S.; supervision, A.V.; project administration, A.V.; funding acquisition, A.V. All authors have read and agreed to the published version of the manuscript.

Funding: This research was funded by the Michael J Fox Foundation for Parkinson Research, grant number 10908, by the Swedish Parkinson Foundation (Parkinsonfonden), grant number 1268/20, by AstraZeneca and AbbVie. Dinahlee Saturnino Guarino was supported by NIH grant U19-NS110456.

Institutional Review Board Statement: The study was approved by the Regional Ethics Committee of Stockholm, Sweden (protocol code 2015/4:6 and date of approval: 17 June 2015).

Informed Consent Statement: Not applicable.

Data Availability Statement: The raw data supporting the conclusions of this article will be made available by the authors upon request.

Acknowledgments: We would like to acknowledge David Holzinger (Translational Sciences, Neuroscience & Ophthalmology Discovery Research, AbbVie Deutschland GmbH & Co., Knollstraße 50, 67061 Ludwigshafen, Germany) for α -syn fibrils generation and Åsa Södergren for technical assistance with autoradiography. All autoradiography experiments were performed at the autoradiography core facility of Karolinska Institutet.

Conflicts of Interest: Charles S. Elmore and Magnus Schou are employed at AstraZeneca. Manolo Mugnaini, Sandra Biesinger, and Sjoerd J. Finnema are employed at AbbVie. Gunnar Nordvall is employed at AlzeCure. Dan Sunnemark is employed at Offspring Biosciences.

Abbreviations

The following abbreviations are used in this manuscript:

A β	amyloid beta
AD	Alzheimer's disease
ARG	autoradiography
α -syn	α -synuclein
CAA	cerebral amyloid angiopathy
CBD	corticobasal degeneration
DLB	dementia with Lewy bodies
IHC	immunohistochemistry
LBD	Lewy-body disease
MSA	multiple-system atrophy
PD	Parkinson's disease
PSP	progressive supranuclear palsy
TMA	tissue microarray

Appendix A

Synthesis of [3 H]GMC-058.

1-(3-bromo-4-methoxyphenyl)-4-(4-nitrophenyl)piperazine.

A suspension of 1-(3-bromo-4-methoxyphenyl)piperazine as the HCl salt (198 mg, 0.64 mmol) and cesium carbonate (524 mg, 1.61 mmol) in DMF (5 mL) was stirred under N₂ as 1-fluoro-4-nitrobenzene (0.075 mL, 0.71 mmol) was added, and the reaction was stirred at 50 °C for 4.5 h and at rt overnight. The reaction was poured into water (30 mL), and the aqueous portion was washed with isopropyl acetate (3 \times 10 mL). The combined organics were dried by passing through a phase separator, and the solvent was removed under reduced pressure. The residue was washed with heptane, and the resultant solid was dried under a vacuum overnight to afford 1-(3-bromo-4-methoxyphenyl)-4-(4-nitrophenyl)piperazine (130 mg, 51.5%) as an orange solid. LCMS (M + H)⁺: 392.1 (100%), 394 (90%). ¹H NMR (500 MHz, DMSO) δ 8.08 (m, 2H), 7.22 (d, J = 2.5 Hz, 1H), 7.09 (m, 2H), 7.01 (m, 2H), 3.77 (s, 3H), 3.60 (m 4H), 3.19 (m, 4H). ¹³C NMR (126 MHz, DMSO) δ 155.1, 149.7, 146.3, 137.5, 126.2, 121.3, 117.1, 113.9, 113.3, 111.6, 56.9, 49.2, 46.7.

4-(4-(3-bromo-4-methoxyphenyl)piperazin-1-yl)aniline.

A suspension of 1-(3-bromo-4-methoxyphenyl)-4-(4-nitrophenyl)piperazine (130 mg, 0.33 mmol) in ethanol (1 mL) and acetic acid (1 mL) was stirred at room temperature under a stream of nitrogen. Iron (130 mg, 2.32 mmol) was added, and the mixture stirred at 80 °C for 90 min and at rt overnight. The mixture was filtered, and the filtrate was diluted with sat. aq. sodium bicarbonate solution. The aqueous portion was washed with ethyl acetate (2 \times 5 mL), and the combined organics were passed through a phase separator. The residue was purified via a reversed-phase HPLC (MeCN/0.2% w/w NH₄OH) to afford an off-white solid (25 mg, 20%). The manipulation of the compound in solution resulted in rapid coloration, so the compound was used immediately in the next reaction. LCMS (M + H)⁺: 362.2 (95%), 364.2 (100%).

N-(4-(4-(3-bromo-4-methoxyphenyl)piperazin-1-yl)phenyl)pivalamide.

A solution of pivaloyl chloride (0.013 mL, 0.10 mmol) and NEt₃ (0.029 mL, 0.21 mmol) in CH₂Cl₂ (1 mL) was stirred for 15 min at rt and then 4-(4-(3-bromo-4-methoxyphenyl)piperazin-1-yl)aniline (25 mg, 0.07 mmol) in CH₂Cl₂ (1 mL) added. The resulting mixture was stirred for 120 min.

Water (5 mL) was added to the reaction mixture and the layers separated. The aqueous layer was washed twice with CH₂Cl₂ (2 × 1 mL), and the combined organic layers passed through a phase separator. The organic layer was concentrated to dryness, and the residue was purified via reversed phase HPLC (35–95% gradient over 7 min). Fractions containing the pure product were combined and lyophilized to afford N-(4-(4-(3-bromo-4-methoxyphenyl)piperazin-1-yl)phenyl)pivalamide (22.00 mg, 71.4%) as an off-white solid. LCMS (M + H)⁺: 446.1 (90%), 448.1 (100%). ¹H NMR (500 MHz, DMSO) δ 8.99 (s, 1H), 7.48 (d, J = 9.1 Hz, 2H), 7.20 (d, J = 2.4 Hz, 1H), 7.01 (m, 2H), 6.93 (d, J = 9.1 Hz, 1H), 3.77 (s, 3H), 3.18 (m, 8H), 1.20 (s, 9H). ¹³C NMR (126 MHz, DMSO): 175.9, 149.0, 147.0, 146.1, 131.7, 121.5, 120.7, 116.5, 115.8, 113.4, 111.1, 56.4, 49.2, 48.9, 27.3.

N-(4-(4-(4-methoxy-[3-³H]phenyl)piperazin-1-yl)phenyl)pivalamide ([³H]GMC-058)

A slurry of N-(4-(4-(3-bromo-4-methoxyphenyl)piperazin-1-yl)phenyl)pivalamide (2.5 mg, 5.60 μmol), 10% Pd-C (2.1 mg, 0.02 mmol) and NEt₃ (20 μL, 0.14 mmol) in DMF (0.5 mL) was degassed using freeze-thaw methodology [22] and T2 (274 GBq, 129 μmol) was added. The reaction mixture was stirred at rt for 4 h. The unused tritium was recovered, and the volatiles were removed by blowing a stream of N₂ over the slurry. MeOH (0.5 mL) was added and removed under a N₂ stream twice. The residue was taken up in EtOH and the catalyst was removed via filtration. HPLC showed 86% radiochemical purity. The residue was purified via preparative HPLC, and product-containing fractions were combined and concentrated to dryness. The residue was taken up in 10 mL of EtOH to give 3554 MBq. LCMS (M – H)[−]: 368.2 (24%), 370.2 (100%). Molar activity: 854 GBq/mmol. ¹H NMR: 9.00 (s, 1H), 7.49 (d, J = 8.5 Hz, 2H), 6.95 (t, J = 10.7 Hz, 4H), 6.86 (s, 1H), 3.71 (s, 3H). ³H NMR: 6.9 (s). LC Rad: 99.5%

Synthesis of [³H]GMC-073.

1-(3-bromo-2-methoxyphenyl)-3-(3-cyano-4-(4-(4-fluorophenyl)piperazin-1-yl)phenyl)urea.

A solution of 5-amino-2-(4-(4-fluorophenyl)piperazin-1-yl)benzotrile (167 mg, 0.56 mmol), 3-bromo-2-methoxyaniline (114 mg, 0.56 mmol), and NEt₃ (0.47 mL, 3.4 mmol) in THF (2 mL) under N₂ was cooled in an ice-bath and was stirred as triphosgene (120 mg, 0.40 mmol) in THF (2 mL) was added. The mixture was stirred for 90 min in the ice-bath. Water (25 mL) was added to the mixture, and the mixture was stirred for 15 min. The sample was diluted with EtOAc, and the organic portion was separated. The aqueous layer was washed with EtOAc, and the combined organics were dried (Na₂SO₄). The solids were removed via filtration, and the solvent was concentrated to dryness. The residue was purified through silica gel chromatography to afford 1-(3-bromo-2-methoxyphenyl)-3-(3-cyano-4-(4-(4-fluorophenyl)piperazin-1-yl)phenyl)urea (34.8 mg, 11.78%) as a pale yellow solid. LCMS (M + 1)⁺: 524.4 (80%), 526.4 (100%) ¹H NMR (500 MHz, DMSO) δ 9.52 (s, 1H), 8.53 (s, 1H), 8.20 (dd, J = 8.3, 1.5 Hz, 1H), 7.91 (d, J = 2.6 Hz, 1H), 7.57 (dd, J = 8.9, 2.7 Hz, 1H), 7.22 (m, 2H), 7.04 (m, 5H), 3.79 (s, 3H), 3.25 (m, 8H).

1-(3-cyano-4-(4-(4-fluorophenyl)piperazin-1-yl)phenyl)-3-(2-methoxy-[3-3H]-phenyl)urea ([3H]GMC-073).

A slurry of 1-(3-bromo-2-methoxyphenyl)-3-(3-cyano-4-(4-(4-fluorophenyl)piperazin-1-yl)phenyl)urea (2.4 mg, 4.58 μmol) and 10% Pd/C (2 mg, 18.79 μmol) in DMF (0.5 mL) and NEt₃ (20 μL , 143.49 μmol) was degassed via two freeze/thaw cycles (1), and T2 (280 GBq, 131 μmol) was added. The reaction mixture was stirred at rt for 4 h. The unused tritium was recovered, and then volatiles were removed by blowing a stream of N₂ over the slurry. MeOH (0.5 mL) was added and removed under a N₂ stream twice. The sample was taken up in 0.5 mL of EtOH and was filtered to yield 4117 MBq. HPLC analysis showed the radiochemical purity to be 47%. The EtOH solution was concentrated to dryness and purified via preparative HPLC. Product-containing fractions were combined and concentrated under vacuum. The sample was dissolved in EtOH (30 mL) to yield 832.8 MBq of [³H]GMC-073. LCMS (M + 1): 446 (19.7%), 448 (100%). Molar activity: 865 GBq/mmol. ¹H NMR (500 MHz, DMSO) δ 9.54 (s, 1H), 8.29 (s, 1H), 8.11 (d, J = 7.9 Hz, 1H), 7.92 (s, 1H), 7.56 (s, 1H), 7.23 (d, J = 9.2 Hz, 1H), 7.10 (s, 2H), 7.05 (s, 2H), 6.91 (s, 1H), 3.89 (s, 3H). ³H NMR (533 MHz, DMSO): 7.08 (d, 4.3 Hz). LC Rad: 98.9%.

Synthesis of [³H]GMC-098.

N-(2-cyano-4'-methoxy-[1,1'-biphenyl]-4-yl)-4-(4-iodophenyl)piperazine-1-carboxamide.

A solution of N-(2-cyano-4'-methoxy-[1,1'-biphenyl]-4-yl)-4-phenylpiperazine-1-carboxamide (10 mg, 24 μmol) and N-iodosuccinimide (12.5 mg, 55.5 μmol) in MeCN (5 mL) was stirred at rt overnight. LCMS analysis showed an incomplete reaction; therefore, N-iodosuccinimide (5 mg, 20 μmol) was added. After 3.5 h, a third portion of N-iodosuccinimide (5 mg, 20 μmol) was added. After a further 90 min, the reaction was concentrated to dryness under a stream of nitrogen, and the residue was purified via preparative HPLC. Product-containing fractions were pooled and lyophilized to afford (1.8 mg, 14%) as a white solid. The location of the iodide was inferred from the tritiation product. LCMS (M + H)⁺: 539.1.

N-(2-cyano-4'-methoxy-[1,1'-biphenyl]-4-yl)-4-([4-3H]phenyl)piperazine-1-carboxamide ([3H]GMC-098).

A slurry of N-(2-cyano-4'-methoxy-[1,1'-biphenyl]-4-yl)-4-(4-iodophenyl)piperazine-1-carboxamide (0.75 mg, 1.4 μmol), 10% Pd-C (1 mg), and NEt₃ (20 μL , 149 μmol) in DMF (0.5 mL) was degassed via two freeze/thaw cycles [23] and T2 (282 GBq, 132 μmol) was added. The reaction mixture was stirred at rt for 4 h. The unused tritium was recovered, and the volatiles were removed by blowing a stream of N₂ over the slurry. MeOH (0.5 mL) was added and removed under a N₂ stream twice. The sample was taken up in 0.5 mL of EtOH and was filtered. HPLC analysis showed the radiochemical purity to be 56%. The EtOH solution was concentrated to dryness, and the residue was purified via preparative HPLC. Product-containing fractions were combined and concentrated under vacuum. The sample was dissolved in EtOH (30 mL) to give 281 MBq of [³H]GMC-098. LCMS (M + H)⁺: 413.3 (8.8%), 415.3 (100%). Molar activity: 974 GBq/mmol. ¹H NMR (500 MHz, DMSO) δ 9.02 (s, 1H), 8.55 (m, 2H), 8.04 (s, 1H), 7.83 (d, J = 8.9 Hz, 1H), 7.49 (m, 3H), 7.23 (m, 3H), 7.07 (d, J = 8.2 Hz, 2H), 7.00 (d, J = 8.2 Hz, 2H). ³H NMR (533 MHz, DMSO): 6.88. LC-RAD 98.5%.

Table A1. Demographic data of cases from the Netherlands Brain Bank selected for the construction of tissue microarrays.

Case n.	Diagnosis	Age	Sex	PMI (h)	Brain Region	A β /pTau/ α -syn *
S11/010	Parkinson's disease	82	M	6.1	Cingulate gyrus	-/+ /+++
S10/47	Lewy-body disease	76	M	6.3	Hippocampus	+++ /+++ /+++
S14/013	Lewy-body disease	68	F	4.6	Hippocampus	+ /+++ /+++
S13/054	Dementia with Lewy bodies	91	F	4.7	Inferior parietal gyrus	+++ /+ /+++
	Multiple-system atrophy	66	M	4.9	Cerebellum	- /- /+++
S10/134	Multiple-system atrophy	65	M	4.75	Cerebellum	- /- /+++
S95/120	Multiple-system atrophy	69	F	4.5	Cerebellum	- /- /+++
S11/074	Corticobasal degeneration	63	M	6.5	Superior frontal gyrus	- /+++ /-
S98/105	Corticobasal degeneration	72	M	5.3	Thalamus and subthalamic nucleus	- /+++ /-
S11/085	Corticobasal degeneration	65	F	6	Thalamus	- /+++ /-
S13/064	Progressive supranuclear palsy	70	M	6.8	Cerebellum	- /+++ /-
S12/004	Progressive supranuclear palsy	65	F	5.8	Cerebellum	- /+++ /-
S12/083	Cerebral amyloid angiopathy	79	M	9.75	Hippocampus	+++ /+++ /-
S98/071	Cerebral amyloid angiopathy	79	M	9.75	Cerebellum	+++ /- /-
S98/071	Cerebral amyloid angiopathy	79	M	9.75	Parietal cortex	+++ /+ /+
S98/071	Non-dementia control	78	F	7.17	Cingulate gyrus	- /- /-
S14/029	Non-dementia control	51	F	7.7	Cingulate gyrus	- /- /-
S94/325	Non-dementia control	63	F	6.4	Cingulate gyrus	- /- /-
S95/258	Non-dementia control	56	M	5.4	Cingulate gyrus	- /- /-
S98/235	Non-dementia control	56	M	5.4	Medial temporal gyrus	- /- /-
S98/235	Non-dementia control	56	M	5.4	Superior frontal gyrus	- /- /-
S98/235	Alzheimer's disease	85	M	4.6	Inferior frontal gyrus	+++ /+++
M05/340	Alzheimer's disease	67	F	5.8	Hippocampus	+++ /+++
M05/332	Alzheimer's disease	88	F	5.2	Hippocampus	+++ /+++
M05/331	Alzheimer's disease	84	F	5.9	Hippocampus	+++ /+++
M05/327	Parkinson's disease	98	M	5.7	Substantia nigra	- /+ /+++
S09/252	Parkinson's disease	78	M	5.8	Substantia nigra	- /+ /+++
S13/059	Parkinson's disease	86	M	4.2	Substantia nigra	+ /- /+++
S13/077	Parkinson's disease	57	M	6.6	Substantia nigra	- /- /+++
S17/055	Parkinson's disease	87	F	7.9	Substantia nigra	- /- /+++
S17/056	Parkinson's disease	90	F	5.3	Substantia nigra	- /+ /+++
S17/101	Parkinson's disease	85	F	5.2	Substantia nigra	+ /+ /+++
S17/162	Parkinson's disease	82	M	6.1	Cingulate gyrus	A β /pTau/ α -syn *

A β /pTau/ α -syn = ICH was performed using antibodies for A β (6E10/4G8), pTau (AT-8), and α -syn (LB509).

* Qualitative score of pathology: - = negative to pathology; + = low abundance of aggregates/inclusions; +++ = high amount of aggregates/inclusions.

Table A2. Demographic data of cases from the Alzheimer’s Disease Research Center selected for brain homogenates.

Diagnosis	Sex(M/F)	Age (years)	PMT (h)	ApoE	A	B	C	Region Sampled
AD	F	88	4	34	3	3	3	MFG
AD	F	67	3	34	3	3	3	MFG
AD	F	81	8	34	3	3	3	MFG
AD	M	61	6	33	3	3	3	MFG
AD	M	62	3	33	3	3	3	MFG
AD	M	84	7	44	3	3	3	MFG
Control	M	44	14.2	n/a	0	0	0	prefrontal, occipital, temporal, parietal.

Table A3. Demographic data of cases from the University of California San Francisco selected for brain homogenates.

Diagnosis	Sex(M/F)	Age (years)	PMT (h)	Abeta Pathology:	Tau Pathology: Specific Tau Lesions	Region Sampled
PSP	M	63	4.4	n/a	Neuronal and glial inclusions, tufted astrocytes	L-SFG
PSP	F	70	7.2	n/a	Neuronal and glial inclusions, tufted astrocytes	L-SFG
PSP	M	68	10.1	n/a	Neuronal and glial inclusions, tufted astrocytes	R-SFG
CBD	M	68	7.4	0	Neuronal and glial inclusions, astrocytic plaques	R-M/IFG(A)
CBD	F	70	7.4	0	Neuronal and glial inclusions, astrocytic plaques	R-M/IFG(A)
CBD	F	63	5.0	0	Neuronal and glial inclusions, astrocytic plaques	R-M/IFG(A)

Table A4. Demographic data of cases from Banner Sun Health Research Institute selected for brain homogenates.

Diagnosis	Sex(M/F)	Age (years)	PMT	LB Stage
PD	M	81	2.5	III. Brainstem/Limbic
PDD	M	70	1.83	III. Brainstem/Limbic
PDD	M	75	2.25	IV. Neocortical
PD	M	75	2.33	IV. Neocortical
MSA-P	F	57	32	n/a.
MSA-P	M	58	12	n/a

Table A5. Compounds displaying K_i values < 30 nM for α -syn and >50 nM for A β and tau. In bold are shown the compounds that were selected for ^3H -radiolabeling.

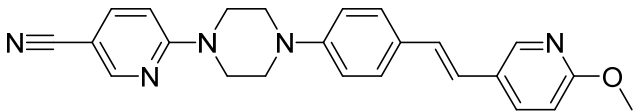
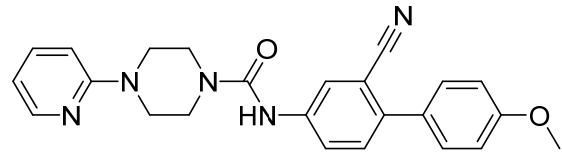
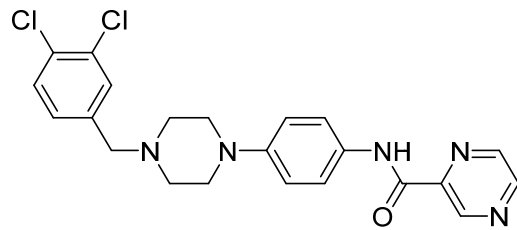
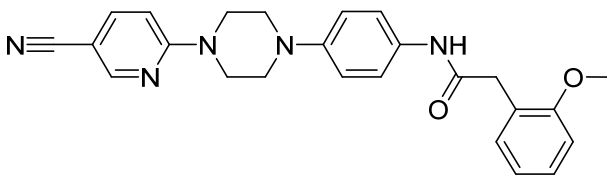
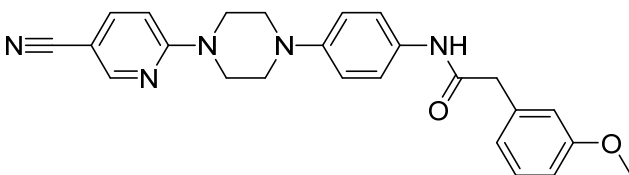
Structure	Name	Molecular Weight	XLogP	α -syn (K_i , nM)	A β (K_i , nM)	Tau-NFT (K_i , nM)
	GMC013_FR-1	397.5	3.37	25.5	63	151
	GMC015	413.5	3.26	28.3	294	761
	GMC021	442.3	2.63	22.2	889	2510
	GMC023	427.5	2.86	21.2	151	44
	GMC024	427.5	2.86	25.3	81	68

Table A5. Cont.

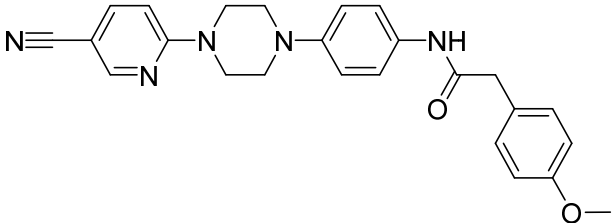
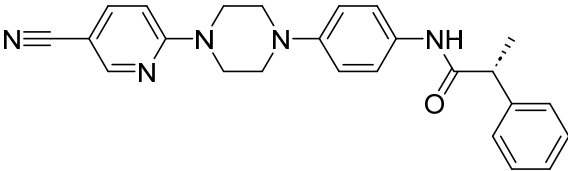
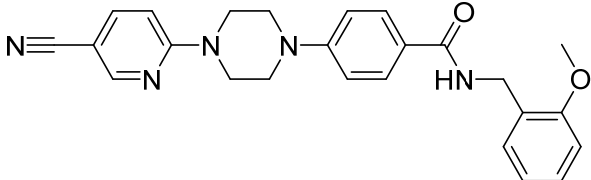
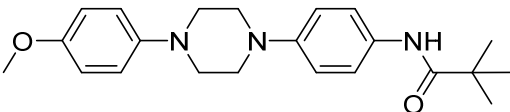
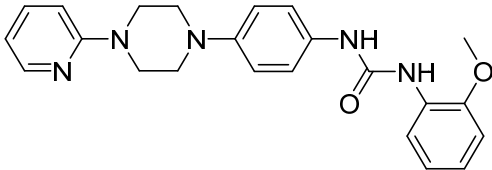
Structure	Name	Molecular Weight	XLogP	α -syn (Ki, nM)	A β (Ki, nM)	Tau-NFT (Ki, nM)
	GMC025	427.5	2.86	29.7	141	50
	GMC044	411.5	3.32	25.2	3440	692
	GMC045	402.5	3.15	24.7	412	239
	GMC058	367.5	3.49	22.5	1490	1320
	GMC070	403.5	2.64	6.8	64	90

Table A5. Cont.

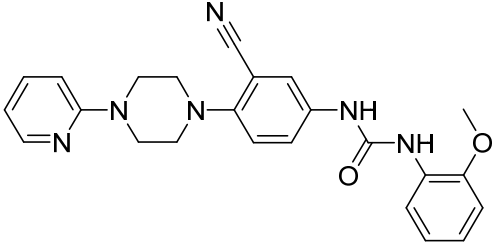
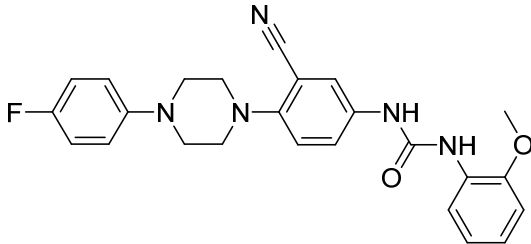
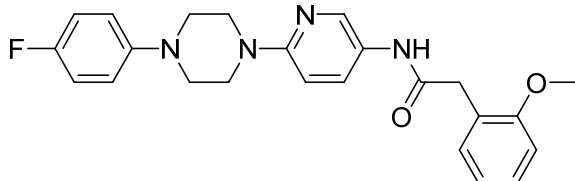
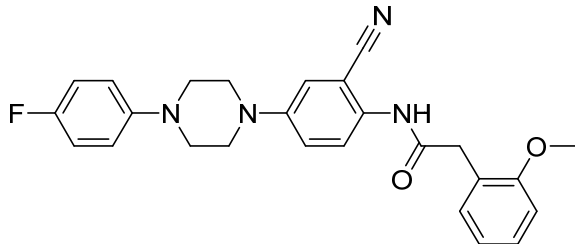
Structure	Name	Molecular Weight	XLogP	α -syn (K _i , nM)	A β (K _i , nM)	Tau-NFT (K _i , nM)
	GMC071	428.5	2.36	14.2	8180	86
	GMC073	445.5	3.37	8.0	2630	248
	GMC079	420.5	3.24	23.9	404	2510
	GMC086	444.5	3.87	15.2	809	26

Table A5. Cont.

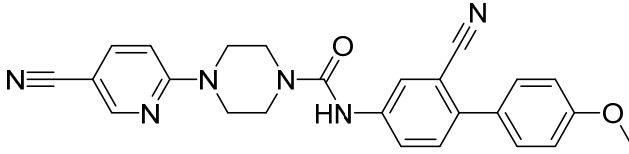
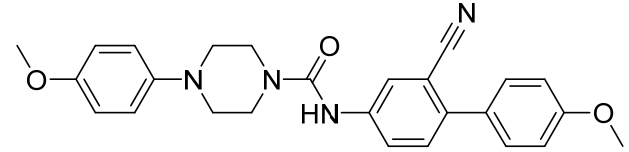
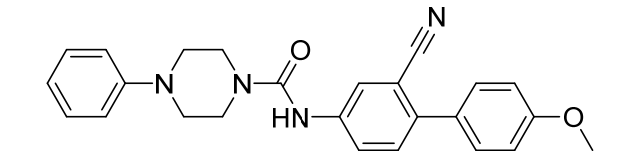
Structure	Name	Molecular Weight	XLogP	α -syn (K _i , nM)	A β (K _i , nM)	Tau-NFT (K _i , nM)
	GMC095	438.5	2.98	14.5	2630	2510
	GMC096	442.5	4.13	6.5	51	2510
	GMC098	442.5	4.13	9.7	226	805

Table A6. Average total, non-specific binding (NSB) and total minus NSB (in fmol/mg tissue equivalent) \pm standard error of the mean (SEM), measured at two concentrations for each radioligand from the gray matter of the cingulate cortex of n = 1 control subject (C03). Average calculated from 4 technical replicates per condition.

	³ H]GMC-058				³ H]GMC-073				³ H]GMC-098			
	25 nM		50 nM		10 nM		20 nM		10 nM		20 nM	
	Total	NSB	Total	NSB	Total	NSB	Total	NSB	Total	NSB	Total	NSB
Average (fmol/mg) \pm SEM	57.6 \pm 1.8	37.6 \pm 3.8	114.1 \pm 9.3	74.6 \pm 4.1	664.6 \pm 24.3	346.9 \pm 14.5	1870 \pm 100.2	1022 \pm 45	2705 \pm 62.2	1878 \pm 74.1	5146 \pm 386.2	2336 \pm 48.5
Total minus NSB (fmol/mg)	20		40		318		848		827		2810	

Table A7. Binding (fmol/mg tissue equivalent) of 25nM [³H]GMC-058 in tissue sections from controls, PD and MSA patients. Each gray matter (GM) or white matter (WM) value represents an average from the ROIs of four replicates.

Condition	Cases	ROI	Binding in fmol/mg		
			Total	NSB (5 μM GMC044)	Total Minus NSB
Non-dementia control (cingulate gyrus)	C01	GM	56.8	60.3	−3.5
		WM	56.9	59.8	−2.9
	C02	GM	44.3	24.6	19.8
		WM	45.3	31.8	13.6
	C03	GM	45.3	28.6	16.7
		WM	48.7	39.0	9.7
MSA (cerebellum)	MSA1	GM	46.9	27.4	19.5
		WM	50.1	33.3	16.8
	MSA2	GM	30.3	19.9	10.3
		WM	52.5	27.7	24.8
PD (cingulate gyrus)	PD1	GM	55.6	42.3	13.3
		WM	52.5	50.6	1.9
	PD2	GM	16.2	17.1	−0.9
		WM	55.4	53.7	1.6
	PD3	GM	59.3	42.0	17.2
		WM	55.4	47.1	8.3

Table A8. Specific 25 nM [³H]GMC058 binding (fmol/mg tissue equivalent) from autoradiography of brain tissue from different proteinopathies. Binding was quantified from gray (GM) and white matter (WM) regions of interest (ROI) in all cases. Bars represent the average ± s.e.m. of two technical replicates quantified from each case. MSA = multiple-system atrophy; CBD = cortical-basal degeneration; PSP = progressive supranuclear palsy; NDE = non-dementia elderly controls. Non-specific binding was measured with excess (5 μM) of cold blocker (GMC-044).

Pathology	Case	Regions	Specific Binding (fmol/mg Tissue Equivalent)	
			Region WM	GM
MSA	MSA3	Cerebellum	21	26
	MSA4		49	23
CBD	CBD1 block 1	SFG	29	50
	CBD1 block 2		130	32
PSP	PSP1	GP	32	102
	PSP2		−1	118
NDE	C03	Cingulate cortex	−2	15
	C04	Caudate	−1	8
	C04	Globus Pallidus	0	10
	Co4	Putamen	4	12

Appendix B

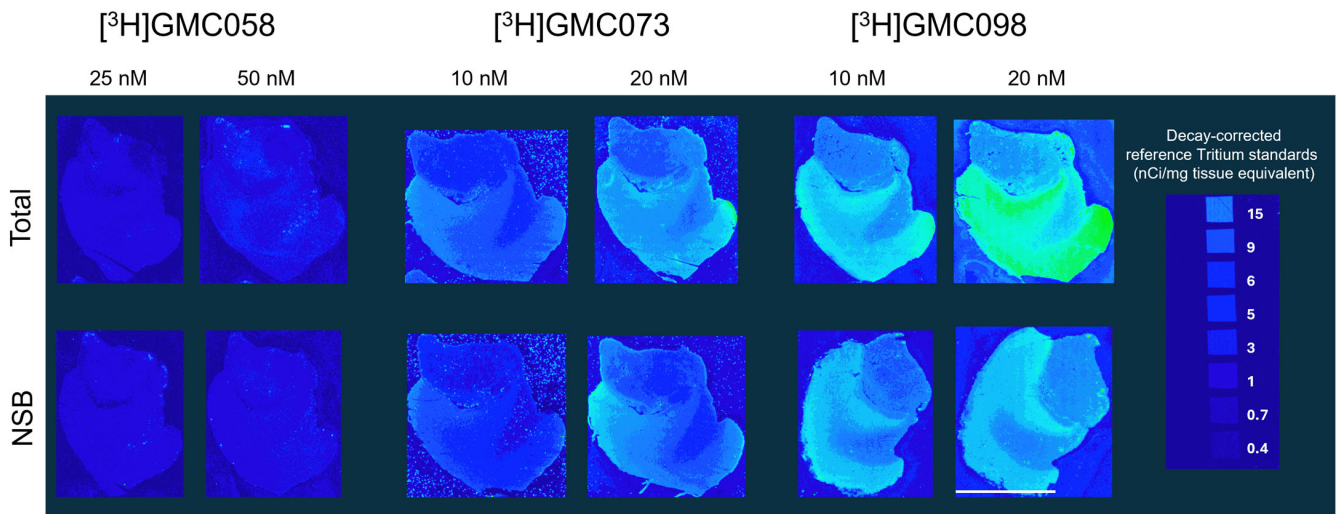


Figure A1. Representative images from a pilot autoradiography experiment on post-mortem sections from the cingulate cortex of one healthy human subject. Testing specific binding of: $[^3\text{H}]\text{GMC-058}$: 25 nM, 50 nM; $[^3\text{H}]\text{GMC-073}$: 10 nM, 20 nM; $[^3\text{H}]\text{GMC-098}$: 10 nM, 20 nM. Non-specific binding (NSB) was measured with excess (5 μM) of blocker GMC044. GMC044 displaced ~65% of $[^3\text{H}]\text{GMC-058}$ binding and ~50% of $[^3\text{H}]\text{GMC-073}$ and $[^3\text{H}]\text{GMC-078}$. Line scale: 10 mm.

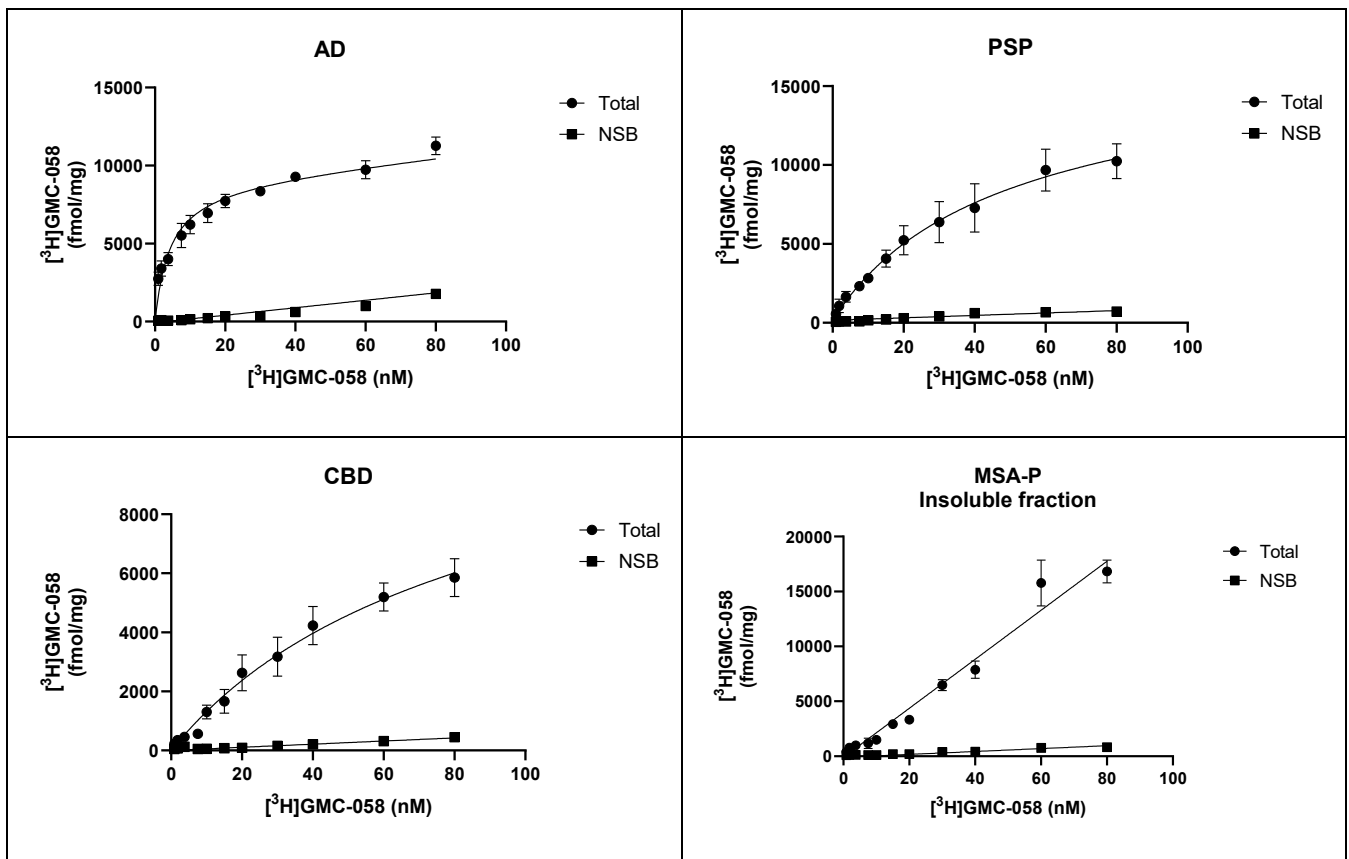


Figure A2. Cont.

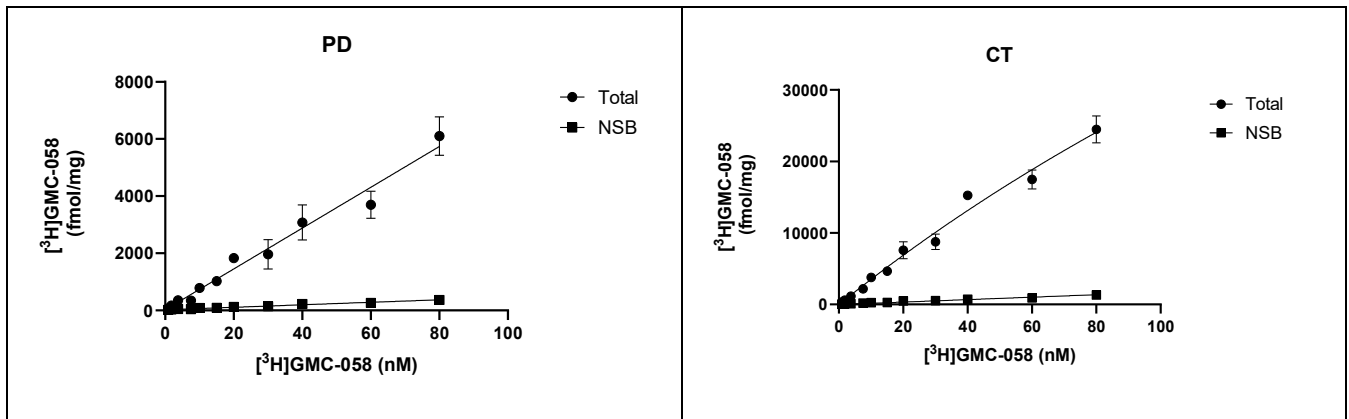


Figure A2. [³H]GMC-058 saturation binding studies. Graphs showing total and non-specific binding of [³H]GMC-058 in homogenates from AD, PSP, CBD, MSA-P, PD, and control patients using concentrations of 0.9 to 80nM.

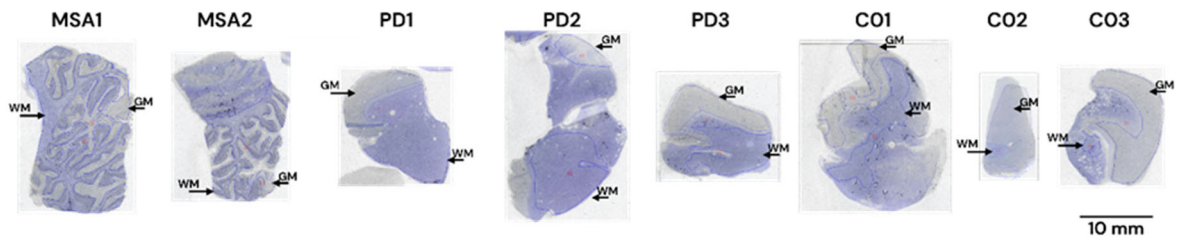


Figure A3. Representative ROIs selected in tissue sections from patients with multiple-system atrophy (MSA), Parkinson’s disease (PD), Lewy-body disease (LBD), and controls (CO) on which analysis was done for Figure 3 and Table A7. The images illustrate an overlay of the toluidine blue stain with the autoradiogram image from the analysis software, where the ROI delineation is visible. The ROIs delineated on the white matter (WM) and gray matter (GM) are indicated with an arrow. Line scale: 10 mm.

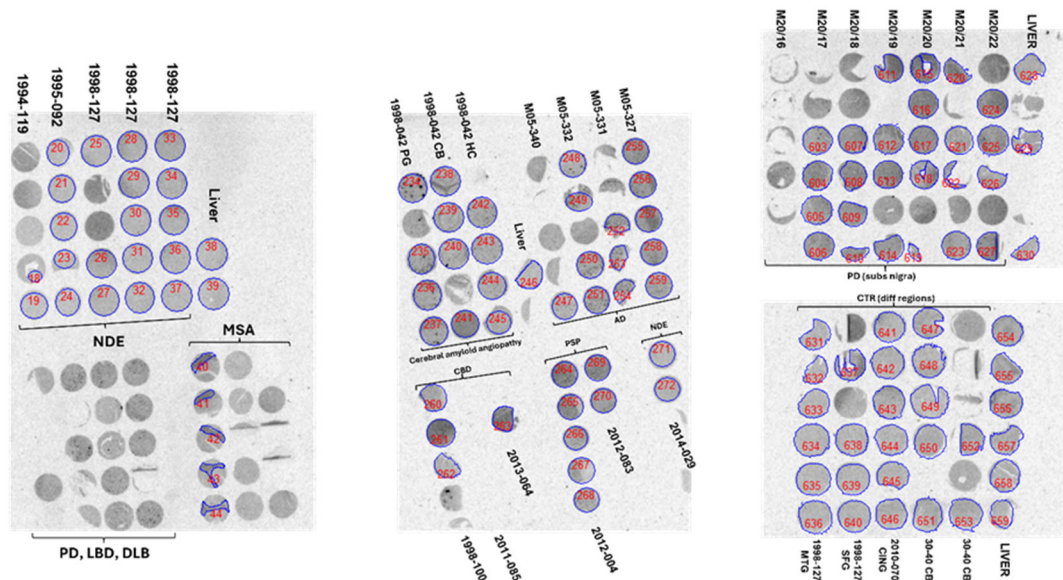


Figure A4. Representative ROIs selected in tissue microarray (TMA) autoradiography on which analysis was done for Table 3, Figures A5 and A6. In the microarrays from PD (substantia nigra), the cores were selected based on the pathological evidence of α -syn inclusions, with no A- β plaques or pTau tangles. In the MSA cases, the ROIs were delineated on the areas where the binding of [³H]GMC-058 was observed and corresponded to areas with α -syn inclusions. The numbers are identifiers of the ROIs generated by the analysis software.

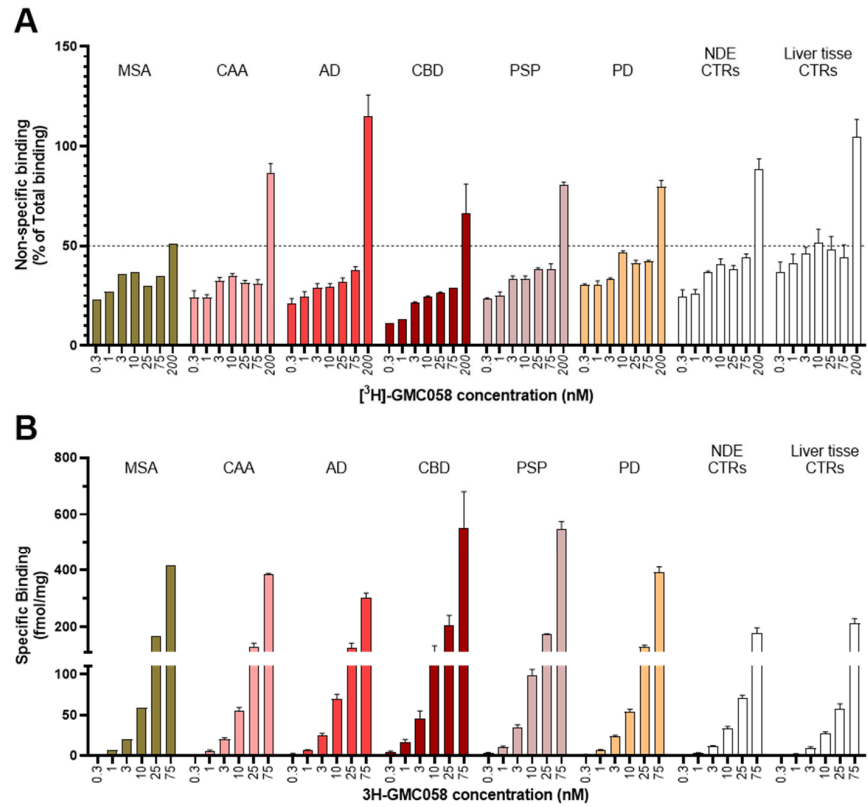


Figure A5. Quantitative analysis from [³H]GMC-058 saturation binding autoradiography in tissue microarrays (TMAs). **(A)** Non-specific binding plotted as % of total binding. **(B)** Specific binding in fmol/mg tissue equivalent. Bars represent the average ± s.e.m. of the respective number of cases as described in Table 2. NDE = non-dementia elderly controls; MSA = multiple-system atrophy; CAA = Cerebral amyloid angiopathy; AD = Alzheimer’s disease; CBD = corticobasal degeneration; PSP = progressive supranuclear palsy; PD = Parkinson’s disease.

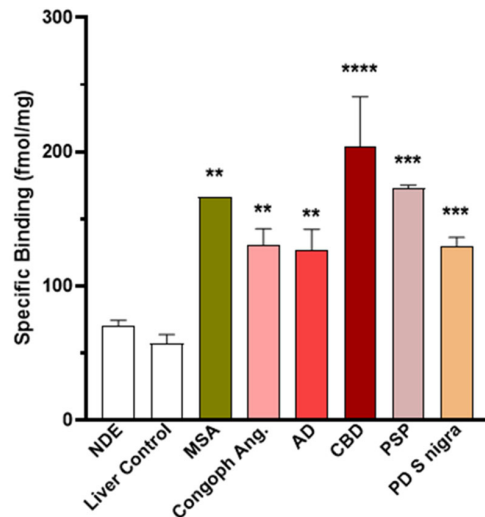


Figure A6. Specific binding (fmol/mg tissue equivalent) of 25 nM [³H]GMC-058, measured in TMAs from cases with different proteinopathies. NDE = non-dementia elderly controls; MSA = multiple-system atrophy; CAA = cerebral amyloid angiopathy; AD = Alzheimer’s disease; CBD = corticobasal degeneration; PSP = progressive supranuclear palsy; PD = Parkinson’s disease. **** *p* < 0.0001; *** *p* < 0.001; ** *p* < 0.01, compared to NDE control, obtained by one-way ANOVA with Dunnett’s multiple comparisons test. Bars represent the average ± s.e.m. of the respective number of cases as described in Table 2. In non-dementia controls (NDE) and liver tissue the values represent displaceable (off-target) binding.

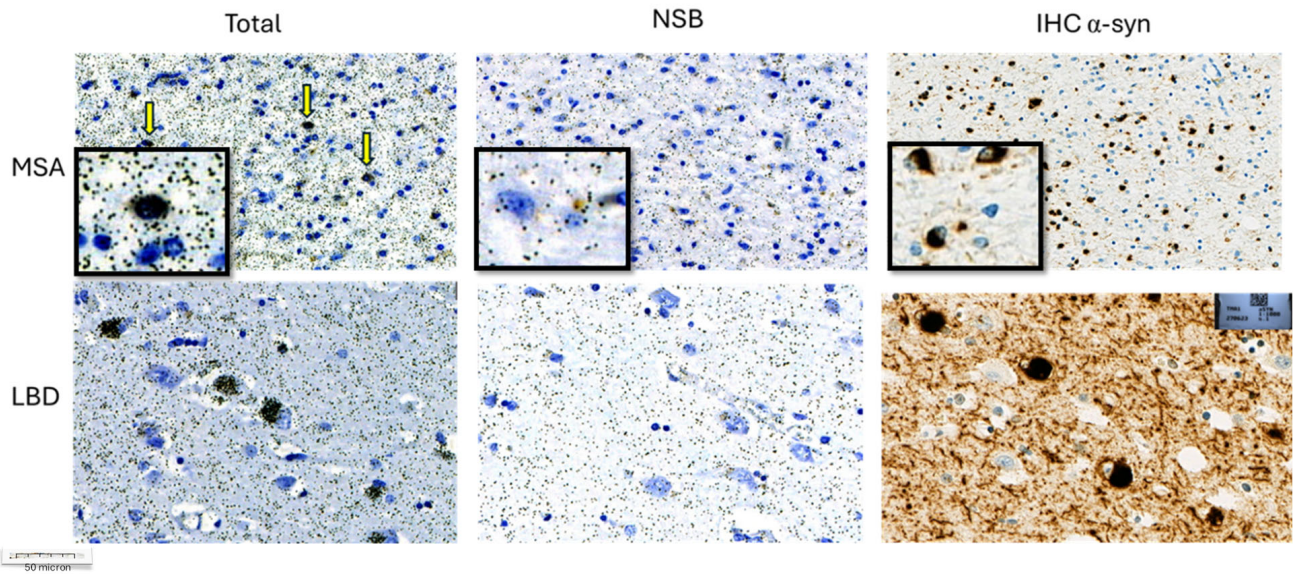


Figure A7. Representative high magnification images from immunohistochemistry (IHC) and emulsion autoradiography (ARG) with 25 nM [^3H]GMC-058 performed on TMA sections from cases with MSA and Lewy-body disease. ARG signal (silver grains on the left) correspond to α -syn inclusions in MSA (oligodendrocytic cytoplasmic inclusions) and PD (Lewy bodies) and is reduced after co-incubation of 5 μM GMC-044.

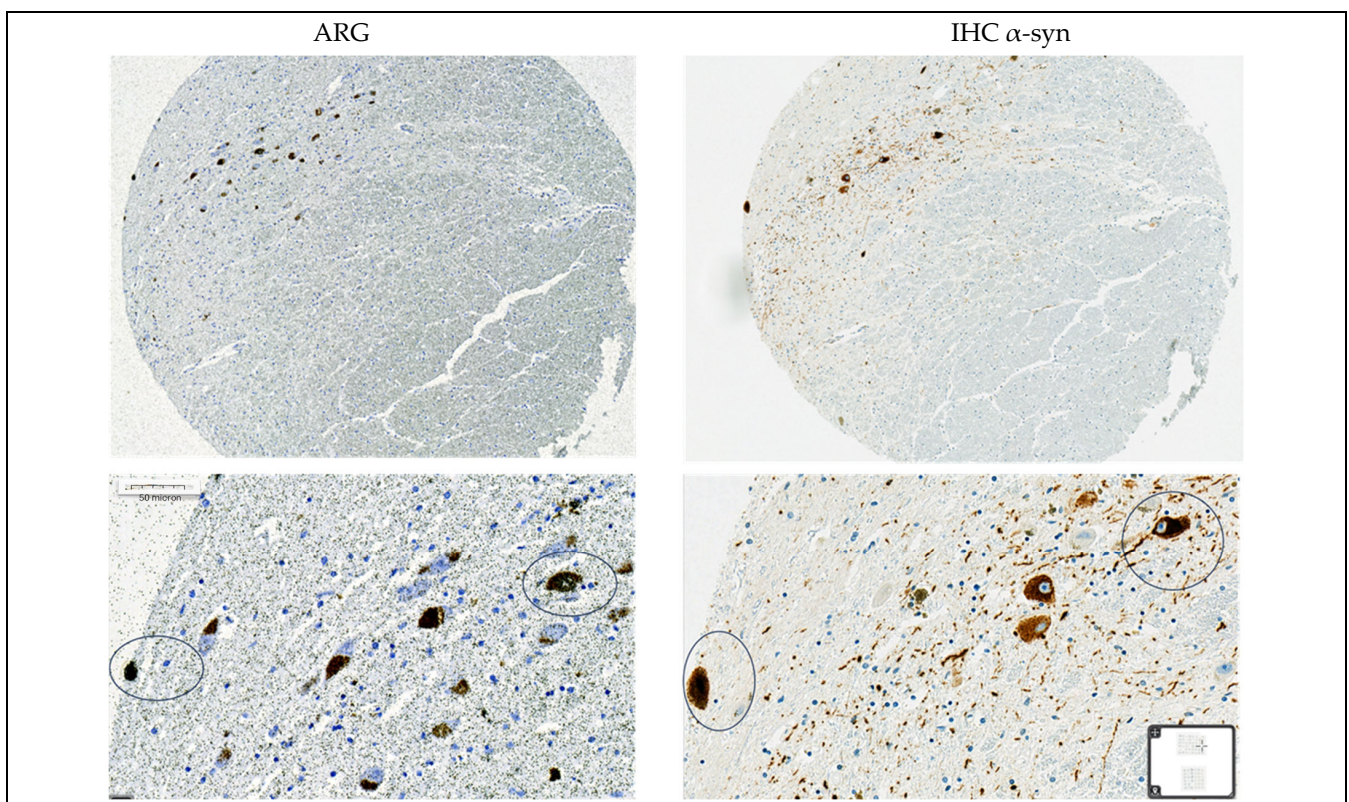


Figure A8. Representative high magnification images from immunohistochemistry (IHC) and emulsion autoradiography (ARG) with 25 nM [^3H]GMC-058 performed on TMA sections from the substantia nigra of one case with Parkinson's disease. The circled Lewy bodies are the same identified with ARG and IHC.

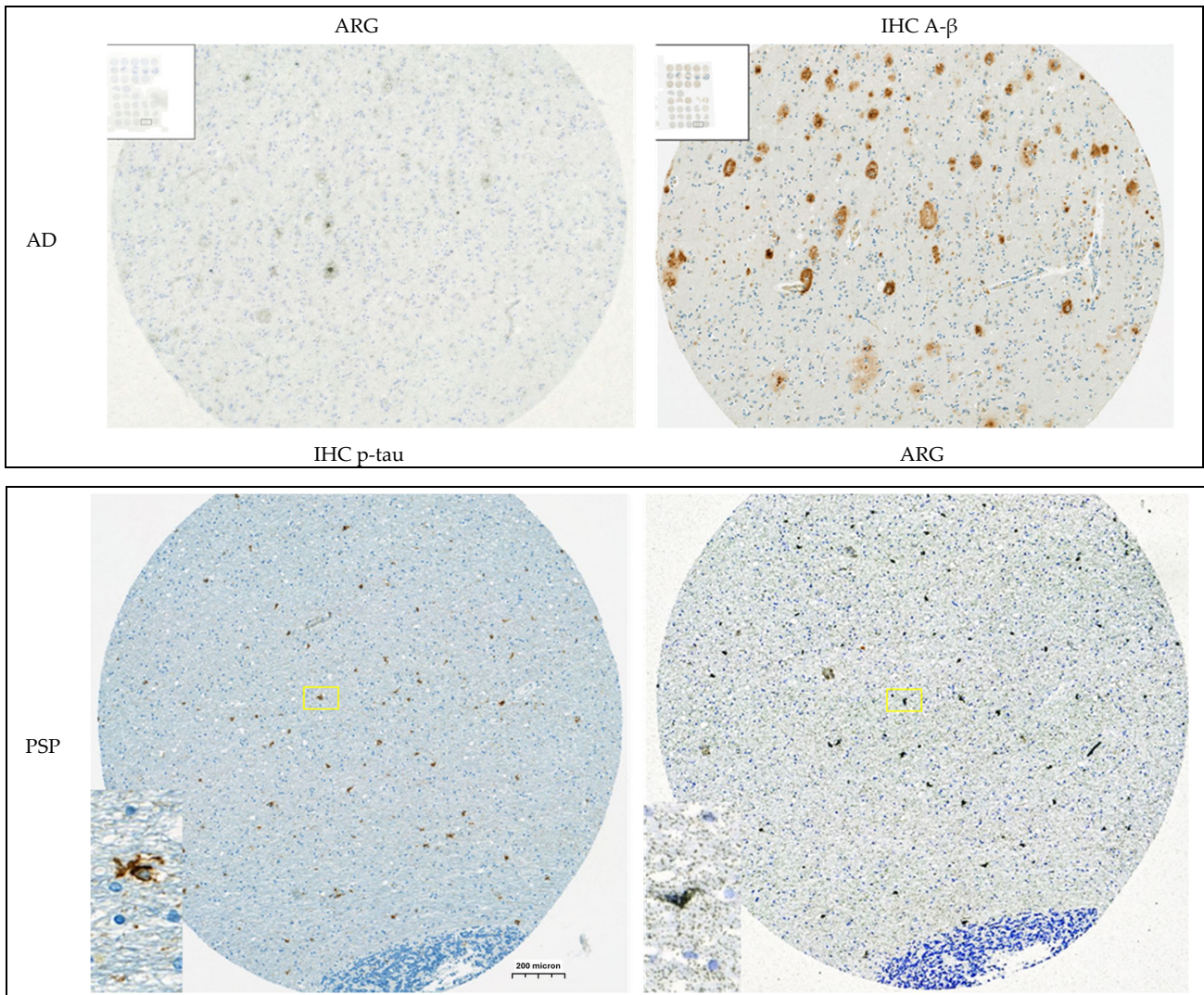


Figure A9. Representative high magnification images from immunohistochemistry (IHC) and emulsion autoradiography (ARG) with 25 nM [^3H]GMC-058 performed on TMA sections from one case with Alzheimer's disease (AD) and one case with progressive supranuclear palsy (PSP). The ARG signal corresponds to dense A- β plaques in AD and p-tau inclusions in PSP.

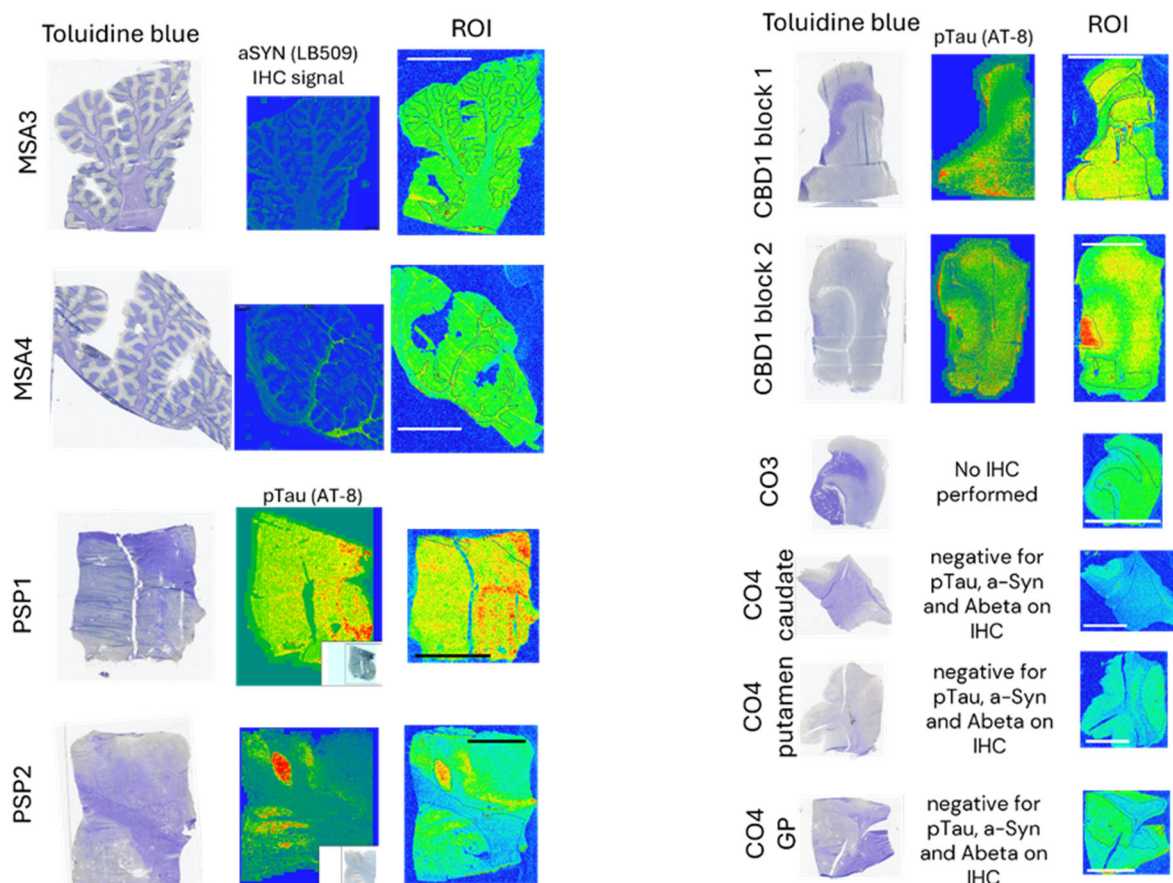


Figure A10. Representative ROIs selected in tissue sections from patients with multiple-system atrophy (MSA), corticobasal degeneration (CBD), progressive supranuclear palsy (PSP), and non-dementia controls (CO) on which analysis was done for Figure 5 and Table A8. ROIs were delineated based on toluidine blue staining for anatomical reference.

References

- McCann, H.; Stevens, C.H.; Cartwright, H.; Halliday, G.M. α -Synucleinopathy phenotypes. *Parkinsonism Relat. Disord.* **2014**, *20* (Suppl. S1), S62–S67. [[CrossRef](#)] [[PubMed](#)]
- Höglinger, G.U.; Adler, C.H.; Berg, D.; Klein, C.; Outeiro, T.F.; Poewe, W.; Postuma, R.; Stoessl, A.J.; Lang, A.E. A biological classification of Parkinson's disease: The SynNeurGe research diagnostic criteria. *Lancet Neurol.* **2024**, *23*, 191–204, ISSN 1474-4422. [[CrossRef](#)] [[PubMed](#)]
- Papp, M.I.; Kahn, J.E.; Lantos, P.L. Glial cytoplasmic inclusions in the CNS of patients with multiple system atrophy (striatonigral degeneration, olivopontocerebellar atrophy and Shy-Drager syndrome). *J. Neurol. Sci.* **1989**, *94*, 79–100. [[CrossRef](#)] [[PubMed](#)]
- Smith, R.; Capotosti, F.; Schain, M.; Ohlsson, T.; Vokali, E.; Molette, J.; Touilloux, T.; Hliva, V.; Dimitrakopoulos, I.K.; Puschmann, A.; et al. The α -synuclein PET tracer [18F] ACI-12589 distinguishes multiple system atrophy from other neurodegenerative diseases. *Nat. Commun.* **2023**, *14*, 6750. [[CrossRef](#)]
- Matsuoka, K.; Ono, M.; Takado, Y.; Hirata, K.; Endo, H.; Ohfusa, T.; Kojima, T.; Yamamoto, T.; Onishi, T.; Orihara, A.; et al. High-Contrast Imaging of α -Synuclein Pathologies in Living Patients with Multiple System Atrophy. *Mov. Disord.* **2022**, *37*, 2159–2161. [[CrossRef](#)] [[PubMed](#)]
- Endo, H.; Ono, M.; Takado, Y.; Matsuoka, K.; Takahashi, M.; Tagai, K.; Kataoka, Y.; Hirata, K.; Takahata, K.; Seki, C.; et al. Imaging α -synuclein pathologies in animal models and patients with Parkinson's and related diseases. *Neuron* **2024**, *112*, 2540–2557. [[CrossRef](#)] [[PubMed](#)]
- Bousset, L.; Pieri, L.; Ruiz-Arlandis, G.; Gath, J.; Jensen, P.H.; Habenstein, B.; Madiona, K.; Olieric, V.; Böckmann, A.; Meier, B.H.; et al. Structural and functional characterization of two alpha-synuclein strains. *Nat. Commun.* **2013**, *4*, 2575. [[CrossRef](#)]
- Gruber, C.C.; Oberdorfer, G.; Voss, C.V.; Kreamsner, J.M.; Kappe, C.O.; Kroutil, W. An Algorithm for the Deconvolution of Mass Spectroscopic Patterns in Isotope Labeling Studies. Evaluation for the Hydrogen-Deuterium Exchange Reaction in Ketones. *J. Org. Chem.* **2007**, *72*, 5778–5783. [[CrossRef](#)]

9. Hostetler, E.D.; Walji, A.M.; Zeng, Z.; Miller, P.; Bennacef, I.; Salinas, C.; Connolly, B.; Gantert, L.; Haley, H.; Holahan, M.; et al. Preclinical characterization of 18F-MK-6240, a promising positron emission tomography (PET) tracer for in vivo quantification of human neurofibrillary tangles (NFTs). *J. Nucl. Med.* **2016**, *57*, 1599–1606. [[CrossRef](#)]
10. Klunk, W.E.; Wang, Y.; Huang, G.F.; Debnath, M.L.; Holt, D.P.; Shao, L.; Hamilton, R.L.; Ikonovic, M.D.; DeKosky, S.T.; Mathis, C.A. The binding of 2-(4'-methylaminophenyl)benzothiazole to postmortem brain homogenates is dominated by the amyloid component. *J. Neurosci.* **2003**, *23*, 2086–2092. [[CrossRef](#)]
11. Zhang, W.; Arteaga, J.; Cashion, D.K.; Chen, G.; Gangadharmath, U.; Gomez, L.F.; Kasi, D.; Lam, C.; Liang, Q.; Liu, C.; et al. A highly selective and specific PET tracer for imaging of tau pathologies. *J. Alzheimers Dis.* **2012**, *31*, 601–612. [[CrossRef](#)] [[PubMed](#)]
12. Bagchi, D.P.; Yu, L.; Perlmutter, J.S.; Xu, J.; Mach, R.H.; Tu, Z.; Kotzbauer, P.T. Binding of the radioligand SII23 to α -synuclein fibrils in Parkinson disease brain tissue establishes feasibility and screening approaches for developing a Parkinson disease imaging agent. *PLoS ONE* **2013**, *8*, e55031. [[CrossRef](#)] [[PubMed](#)] [[PubMed Central](#)]
13. Stehouwer, J.S.; Huang, G.; Guarino, D.S.; Debnath, M.L.; Polu, A.; Geib, S.J.; Lopresti, B.; Ikonovic, M.D.; Mason, N.; Mach, R.H.; et al. Structure-Activity Relationships and Evaluation of 2-(Heteroaryl-cycloalkyl)-1H-indoles as Tauopathy Positron Emission Tomography Radiotracers. *J. Med. Chem.* **2025**, *68*, 6462–6492. [[CrossRef](#)] [[PubMed](#)] [[PubMed Central](#)]
14. Miranda-Azpiazu, P.; Svedberg, M.; Higuchi, M.; Ono, M.; Jia, Z.; Sunnemark, D.; Elmore, C.S.; Schou, M.; Varrone, A. Identification and in vitro characterization of C05-01, a PBB3 derivative with improved affinity for alpha-synuclein. *Brain Res.* **2020**, *1749*, 147131. [[CrossRef](#)] [[PubMed](#)]
15. Lund, H.; Cowburn, R.F.; Gustafsson, E.; Strömberg, K.; Svensson, A.; Dahllund, L.; Malinowsky, D.; Sunnemark, D. TTBK1 in Alzheimer's Disease Brain. *Brain Pathol.* **2012**, *23*, 378–389. [[CrossRef](#)]
16. Aguero, C.; Dhaynaut, M.; Amaral, A.C.; Moon, S.-H.; Neelamegam, R.; Scapellato, M.; Carazo-Casas, C.; Kumar, S.; El Fakhri, G.; Johnson, K.; et al. Head-to-head comparison of [18F]-Flortaucipir, [18F]-MK-6240 and [18F]-PI-2620 postmortem binding across the spectrum of neurodegenerative diseases. *Acta Neuropathol.* **2024**, *147*, 25. [[CrossRef](#)] [[PubMed](#)] [[PubMed Central](#)]
17. Mueller, A.; Bullich, S.; Barret, O.; Madonia, J.; Berndt, M.; Papin, C.; Perrotin, A.; Koglin, N.; Kroth, H.; Pfeifer, A.; et al. Tau PET imaging with 18F-PI-2620 in Patients with Alzheimer Disease and Healthy Controls: A First-in-Humans Study. *J. Nucl. Med.* **2020**, *61*, 911–919. [[CrossRef](#)] [[PubMed](#)] [[PubMed Central](#)]
18. Tagai, K.; Ono, M.; Kubota, M.; Kitamura, S.; Takahata, K.; Seki, C.; Takado, Y.; Shinotoh, H.; Sano, Y.; Yamamoto, Y.; et al. High-Contrast In Vivo Imaging of Tau Pathologies in Alzheimer's and Non-Alzheimer's Disease Tauopathies. *Neuron* **2021**, *109*, 42–58.e8. [[CrossRef](#)] [[PubMed](#)]
19. Brendel, M.; Barthel, H.; Van Eimeren, T.; Marek, K.; Beyer, L.; Song, M.; Palleis, C.; Gehmeyr, M.; Fietzek, U.; Respondek, G.; et al. Assessment of 18F-PI-2620 as a Biomarker in Progressive Supranuclear Palsy. *JAMA Neurol.* **2020**, *77*, 1408–1419, *Erratum in JAMA Neurol.* **2020**, *77*, 1453. [[CrossRef](#)] [[PubMed](#)] [[PubMed Central](#)]
20. Li, L.; Liu, F.; Li, M.; Lu, J.; Sun, Y.; Liang, X.; Bao, W.; Chen, Q.; Li, X.; Zhou, X.; et al. Clinical utility of 18F-APN-1607 tau PET imaging in patients with progressive supranuclear palsy. *Mov. Disord.* **2021**, *36*, 2314–2323. [[CrossRef](#)]
21. Lindberg, A.; Murrell, E.; Tong, J.; Mason, N.S.; Sohn, D.; Sandell, J.; Ström, P.; Stehouwer, J.S.; Lopresti, B.J.; Viklund, J.; et al. Ligand-based design of [18F]OXD-2314 for PET imaging in non-Alzheimer's disease tauopathies. *Nat. Commun.* **2024**, *15*, 5109. [[CrossRef](#)] [[PubMed](#)] [[PubMed Central](#)]
22. Kim, H.Y.; Chia, W.K.; Hsieh, C.-J.; Saturnino Guarino, D.; Graham, T.J.A.; Lengyel-Zhand, Z.; Schneider, M.; Tomita, C.; Lougee, M.G.; Kim, H.J.; et al. A Novel Brain PET Radiotracer for Imaging Alpha Synuclein Fibrils in Multiple System Atrophy. *J. Med. Chem.* **2023**, *66*, 12185–12202. [[CrossRef](#)] [[PubMed](#)]
23. Shriver, D.F.; Drezdson, M.A. *The Manipulation of Air-Sensitive Compounds*; John Wiley and Sons, Inc.: New York, NY, USA, 1986; p. 104, ISBN 978-0-471-86773-9.

Disclaimer/Publisher's Note: The statements, opinions and data contained in all publications are solely those of the individual author(s) and contributor(s) and not of MDPI and/or the editor(s). MDPI and/or the editor(s) disclaim responsibility for any injury to people or property resulting from any ideas, methods, instructions or products referred to in the content.